



國立臺灣大學電機資訊學院光電工程學研究所

碩士論文

Graduate Institute of Photonics and Optoelectronics  
College of Electrical Engineering and Computer Science

National Taiwan University

Master Thesis

二維光子晶體發光二極體結合量子點材料之光通訊系

統分析

Two-dimensional Photonic Crystal Light-emitting Diodes

Combined with Quantum Dots for Visible Light

Communication System Analysis

蔣文皓

Wen-Hao Chiang

指導教授：黃建璋 博士

Advisor: Jian-Jang Huang, Ph.D.

中華民國 111 年 9 月

September 2022

# 口試委員審定書



國立臺灣大學碩士學位論文

口試委員會審定書

二維光子晶體發光二極體結合量子點材料之  
光通訊系統分析

Two-dimensional Photonic Crystal Light-emitting  
Diodes Combined with Quantum Dots for Visible  
Light Communication System Analysis

本論文係蔣文皓君（學號 R09941063）在國立臺灣大學  
光電工程學研究所完成之碩士學位論文，於民國 111 年 8 月  
18 日承下列考試委員審查通過及口試及格，特此證明

口試委員：

黃建瑋

（指導教授）

林孝如

林建中

鄭浩中

所 長

吳育任



## 致謝

生命稍縱即逝，過去認為成績代表一切，不斷的再應付考試，答案都在書上都能迎刃而解，然而到了碩士班期間，並不能向過往一樣，需要的是獨立的思考，自己的想法，經過這兩年磨練，我也學習解決問題的能力，不過這也只是入社會前的基本訓練，畢業後進入職場將面臨更嚴峻的考驗，因此這兩年的歷練過程很值得我省思，為將來的我建立良好的基礎。

首先，非常感謝教授您在兩年前願意收我進實驗室，不僅在製程及量測上給我許多建議，並教導我如何撰寫完整的計畫書，針對每個小細節仔細修正，讓我獲益良多，在時間有限的情況下，我相信這兩年的收穫必定能為將來的我，不管是工作、家庭還是其他方面，都能有所幫助！

非常謝謝博士班學長岱頡，與我分享許多經驗，在製程實驗也會一同帶我操作，報告方面也提供許多建議，不僅讓我事半功半，也讓我學習許多，每到 312，都會看到那熟悉的背影，為生活增添許多樂趣，從不枯燥乏味。

也感謝學弟宇翔和弘毅，有他們一同實驗的陪伴，減少些孤獨感，並在我畢業前夕最忙的時候能獨自承接計畫的重責大任，幫助我分擔事情，讓我能更專注於自己的研究，未來肯定能成為 LED 組的扛霸子！感謝我的學長學弟妹

謝謝庚益、溢愷、旭慶及育資，有幸能夠在研究所期間一起奮鬥，兩年之間也會互相提供建議並討論實驗上的問題，碰到狀況也會互相幫忙，讓我們一同度過難關，未來你們一定也能在工作上有一番成就。

再者，也要感謝我的女友惟茜，即使我們在不同的實驗室各自忙碌，也會騰出空檔互相談心聊天，一路上的陪伴，不曾讓我感受到孤單，豐富了我的生活。最後也最重要感謝我的爸媽，在生活上無微不至的照顧，讓我能夠更專注於學業與研究，在我心情低迷的時候也會適時的給予鼓勵，提振精神。在實驗室經歷的大小事仍歷歷在目，這些經驗都將成為我的養分，最後再次感謝 JLAB 大家庭！



## 摘要

可見光通訊系統近來年逐漸興起，逐漸應用在我們的日常生活中，無線通訊結合一般照明系統，使得這樣的組合成為具有潛力的通訊系統。對於無線通訊的需求漸漸增加，元件操作速率的提升也成為重要的目標。藍光發光二極體 (LED) 仍是目前最主要的發光源，同時也作為白色發光元件的發光源之一，但其較長的自發性輻射複合生命週期影響整體調變頻寬，因此除了提升 LED 操作速率外，結合量子點探討元件反應速率為本論文主要目標。

一般而言，縮小 LED 元件尺寸，雖然可提升元件的頻寬，但也減少了整體發光面積與強度。本論文將藍光 LED 結合二維光子晶體結構，透過此結構提升頻寬，針對開關鍵控調變的方式下，以 178 MHz 的調變頻寬，成功達到資料傳輸率 400 Mbps，因此在我們的實驗下證實，利用氮化鎵系之藍光 LED 作為發光元件，並加入二微光子晶體結構，可成功提升元件的調變頻寬。

LED 結合多樣的顏色轉換技術已被廣泛的使用在可見光通訊，但量子點參雜在奈米洞內的電光頻率響應卻很少討論。此篇文章我們提出 LED 結合光子晶體結構和綠光的量子點用於研究頻率響應。當考慮到整體藍光與綠光混和後的輸出信號時，我們觀察到具有量子點的光子晶體 LED，其調變質量優於具有量子點的傳統 LED。然而，當只有量子點所轉換綠光的頻率響應則顯示出矛盾的結果。較慢的電光轉換響應歸因於在光子晶體 LED 上的量子點的輻射和非輻射能量轉移過程產生更多的路徑來轉換至綠色量子點發光。


關鍵字：發光二極體、可見光通訊、光子晶體、頻率響應、量子點、螢光共振能量轉移

# ABSTRACT



Visible light communication technologies have steadily arisen in recent years and are gradually being used in our daily lives. The combination of wireless communication and general lighting systems could be used as a communication system. Blue light-emitting diodes (LEDs) continue to be the most significant light-emitting sources, and they are also one of the light-emitting sources of white light-emitting components, although their long spontaneous radiation recombination lifetime limits the total modulation bandwidth. As a result, in addition to increasing the operating speed of LEDs, the major purpose of this thesis is to explore the device's E-O (electro-optical) response when combined with quantum dots.

In general, shrinking the size of an LED mesa may enhance its bandwidth while simultaneously decreasing its total light-emitting area and intensity. In our study, a two-dimensional photonic crystal (PhC) structure is embedded in the blue LEDs (PhCLEDs), which improves the optical bandwidth. With on-off keying modulation and a modulation bandwidth of 178 MHz, a data transmission rate of 400 Mbps is successfully achieved. In our experiments, it has been shown that the modulation bandwidth of the elements can be successfully increased by using GaN-based blue LEDs with a two-dimension photonic crystal structure.



Though light-emitting diodes (LEDs) combined with various color conversion techniques have been widely explored for VLC (visible light communication), E-O (electro-optical) frequency responses of devices with quantum dots (QDs) embedded within the nanoholes have rarely addressed. Here we propose LEDs with embedded photonic crystal (PhC) nanohole patterns and green light QDs for studying E-O frequency bandwidths. We observe the E-O modulation quality of PhC LEDs with QDs is better than a conventional LED with QDs when the overall blue mixed with green light output signal is considered. However, the optical response of only QD converted green light shows a contradictory result. The slower E-O conversion response is attributed to multi-path green light generation from both radiative and nonradiative energy transfer processes for QDs coated on the PhC LEDs.

Key word: light-emitting diode, visible light communication, photonic crystals, electro-optical frequency response, colloidal quantum dot, Förster resonance energy transfer.

# CONTENTS



口試委員審定書 .....	i
致謝 .....	ii
摘要 .....	iii
ABSTRACT .....	iv
CONTENTS .....	vi
LIST OF FIGURES .....	viii
LIST OF TABLES .....	xi
<b>Chapter 1. Introduction .....</b>	<b>1</b>
1.1 Overview of Visible Light Communication .....	1
1.2 Motivation .....	4
1.3 Thesis Outline.....	7
<b>Chapter 2. Background of High-Speed Modulation of Two-dimensional Photonic Crystal GaN LEDs.....</b>	<b>8</b>
2.1 Background of Photonic Crystal LEDs .....	8
2.2 Process Flow of Photonic Crystal LEDs .....	11
2.3 Characteristics of the DC Feature.....	13
2.4 Electro-Optical Behavior of PhCLEDs .....	15
2.5 On-off Keying (OOK) Technique.....	18
2.6 PhCLEDs with Digital Modulation .....	19
2.7 Summary.....	23
<b>Chapter 3. Quantum Dots Integrated with Photonics Crystal LED for Visible Light Communication .....</b>	<b>24</b>
3.1 Background of Quantum Dots.....	24



3.2	Colloidal Quantum Dots.....	25
3.3	Förster Resonance Energy Transfer.....	27
3.4	Process Flow of PhCLEDs with Quantum Dots.....	29
3.5	Characteristics of the DC Feature of Conventional LEDs and PhCLEDs	
	33	
3.6	Emission Spectra of LEDs with QDs .....	35
3.7	Electro-to-optical Response Performance .....	39
3.8	LEDs Integrated with QDs for Digital Modulation.....	42
3.9	E-O Response Performance of LED Integrated with only Green QDs	
	45	
3.10	Summary.....	49
<b>Chapter 4.</b>	<b>Conclusion .....</b>	<b>50</b>
<b>Reference .....</b>		<b>52</b>



# LIST OF FIGURES



Fig. 2.1 3rd-order  $\Gamma$ M diffraction by PhCs with a 520 nm-period hexagonal lattice.

Three diffraction angles for 450 nm wavelength extracted modes were determined.

..... 10

Fig. 2.2 Process Flow of PhCLEDs ..... 11

Fig. 2.3 (a) A schematic drawing of a PhCLED's cross-section. (b) The micro picture of

a 5mA LED current. (c) SEM photograph of a photonic crystal patterns. .... 12

Fig. 2.4 Electroluminescence spectra of PhC-80 and C-80. .... 14

Fig. 2.5 L-I-V curves of (a) PhC-120 and C-120, and (b) PhC-80 and C-80. .... 14

Fig. 2.6 Experimental configuration of the frequency response system. .... 15

Fig. 2.7 Optical frequency responses of CLEDs and PhCLEDs with the mesa size of (a)

$120 \times 120 \mu\text{m}^2$  (b)  $80 \times 80 \mu\text{m}^2$  under 40mA current injection. .... 17

Fig. 2.8 Small-signal equivalent model of LEDs with RF probe pads. .... 17

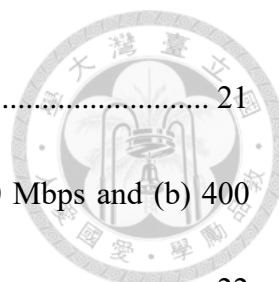
Fig. 2.9 (a) A non-return-to-zero binary code (b) The eye diagram pattern ..... 18

Fig. 2.10 Setup for measuring of the OOK modulation system. .... 20

Fig. 2.11 Eye diagrams of (a) C-80 and (b) PhC-80 at data rates of 100Mbps, 200Mbps,

and 400Mbps. .... 21

Fig. 2.12 SNR performance of the PhC-80 and C-80 at various transmission data rates.



..... 21

Fig. 2.13 BER curves for PhC-80 and C-80 at data rates of (a) 200 Mbps and (b) 400 Mbps..... 22

Fig. 3.1 Process flow of lateral PhCLED ..... 30

Fig. 3.2 (a) Schematic and structure of the PhCLED. (b) SEM image of the PhCs nanohole arrays. .... 31

Fig. 3.3 Schematic diagram of (a) QD-PhCLED, (b) QD-CLED. In this work, QD-CLEDs have three different QD coating thicknesses. .... 32

Fig. 3.4 L-I-V curves of PhCLED and CLED. .... 34

Fig. 3.5 Output spectra of (a) PhCLEDs with and without QDs, (b) CLED and QC-CLED-A. (c) Normalized output spectra of CLEDs with different QDs thickness. (d) Comparison of green to blue light ratio. The blue light output intensity is normalized to 1 for comparisons ..... 37

Fig. 3.6 (a) Illustration of the FRET process between the MQW in the PhCLED and QD. (b) Energy transfer paths for the QD-PhCLED and QD-CLED. .... 37

Fig. 3.7 Enlargement and normalization of the green light emission peak in Fig. 3.5... 38

Fig. 3.8 Setup for frequency response system. .... 40

Fig. 3.9 Comparison of frequency responses between QD-PhC-LED and QD-CLEDs. 41

Fig. 3.10 The evaluated eye diagrams of (a) QD-PhCLED, (b) QD-CLED-A, (c) QD-

CLED-B and (d) QD-CLED-C. (e) The SNR performance of devices at different data rates. .... 44

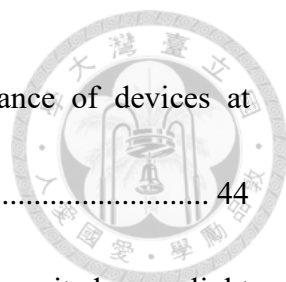


Fig. 3.11 (a) Comparison of frequency responses between only QDs excited green light in QD-PhCLED and QD-CLEDs. (b) Schematic of energy transfer path between QD-PhCLED and QD-CLED. .... 47

Fig. 3.12 (a) TRPL decay profiles of QD-PhCLED and QD-CLEDs. (b) Schematic of re-absorption and FRET process in QDs. .... 48

# LIST OF TABLES



Table 1.1 The demand for mobile data traffic per month. .... 2

# Chapter 1. Introduction



## 1.1 Overview of Visible Light Communication

In the past few years, due to the exponential development of internet data traffic, the need for high-speed data transmission is increasing. By 2023, 110 exabytes per month of mobile data traffic is expected, which is roughly three times the growth expected in 2020 [1]. Visible light communication (VLC), which uses the visible light spectrum (370nm to 780nm) developed for illumination as an alternative sub-GHz wireless transmission option, has gained popularity in recent years due to the rise of solid-state lighting (SSL) [2].

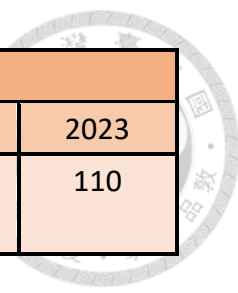
VLC is a subtype of optical wireless communication (OWC) technology that has various advantages [3]. There are severe regulations and limitations on the RF spectrum, whereas the visible light spectrum is widely available and inexpensive to operate [4]. Similarly, the VLC system's high level of security is due to its non-penetrating transmission and is typically used for interior communication. Similarly, the VLC system's high level of security is due to its non-penetrating transmission and is typically used for interior communication. Additionally, VLC is referred as "green communication." To provide light in our daily life, light emitting diodes (LEDs) have become extensively adopted for use. Adding LEDs and signal transmitters to the VLC

system appears to be the most promising option. Consequently, the goal of this thesis is to build LEDs with innovative architectures for both optical transmitters and illumination.

The VLC system must expand the VLC link's capacity within the restricted bandwidth of LEDs in order to deal with the amounts of data being transmitted. For high-speed data transmission, several modulation schemes have been researched in RF communication. Orthogonal frequency-division multiplexing (OFDM) schemes with pre- and post-equalization techniques were employed and achieved 3 Gbit/s transmission through the use of digital modulation methods such on-off keying (OOK) at speeds up to 1.7 Gbit/s [5]. The VLC system has also been widely implemented and advised to use multilayer pulse amplitude modulation (m-PAM) and pulse position modulation (PPM) approaches [6].

What's more, for high-speed data transfer, white light communication is becoming increasingly important. However, the combination of blue LEDs and the limited bandwidth of these phosphor-based emitters have low bandwidth, which restricts the highest data transfer speed that may be achieved [7]. Colloidal quantum dots (QDs) as a potential color conversion material has developed to demonstrate flexible emission, limited luminescent spectra, and high quantum yield in order to expand the bandwidth of white light systems [8, 9].

Table 1.1 The demand for mobile data traffic per month.



Monthly traffic in exabytes					
Year	2019	2020	2021	2022	2023
Mobile data traffic (exabytes)	28.5	40.7	56.80	77.5	110

## 1.2 Motivation



GaN-based LEDs have been shown to be advantageous as the transmitter of a VLC system in recent studies. These benefits include stable optical output power and excellent carrier confinement [8]. Nevertheless, the bandwidth constraint of LEDs often prevents their usage in radio frequency (RF) applications. There have been reported and tested methods for enhancing the modulation bandwidth. In order to achieve a high enough signal-to-noise ratio (SNR) for reliable data transmission, micro-LEDs ( $\mu$ -LEDs) with a flip-chip architecture may minimize the device's resistance-capacitance (RC) delay while maintaining a high enough optical output power [10, 11]. For its short radiative recombination lifetime, resonant-cavity light-emitting diodes (RCLEDs) may generate coherent light and improve the Purcell effect [12].

The photon lifetime of the stimulating emission in optical communications is the primary distinction between lasers and LEDs when used as optical emitters in a VLC system. To combine the communication and light source, LEDs must have enough light output power and cost less than other devices. In order to increase the emission rate with a much shorter radiative recombination lifetime, we first presented a revolutionary design of the LED structure in this thesis, employing a sapphire substrate and integrated LEDs with photonic crystal (PhC) structures. In this work, we used blue-light LEDs for

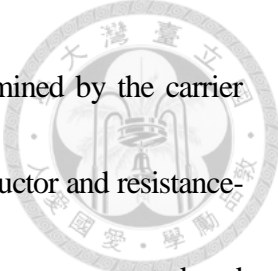




VLC applications since practically all commercial LEDs for lighting are based on blue LEDs mixed with yellow phosphor. PhCLEDs' small- and large-signal modulation potential for VLC was studied.

Traditionally, white light is the most commonly used indoor lighting, composed of LED (light-emitting diode) generated blue light and phosphor-converted yellow light. The data transmission bandwidth using such a white light source is limited by phosphor [10, 11]. Recently, with the rapid development of various types of colloidal quantum dots (QDs), color conversion from by QDs has widely been explored for solid-state lighting and micro-LED displays [12, 13]. The E-O conversion bandwidth and the quality of large-signal transmission using blue LEDs combined with QDs for VLC were thus studied by many researchers [9, 14, 15]. For example, the optical bandwidth of blue LEDs with QDs was compared with blue LEDs with yellow phosphors. A bandwidth increase from 1.7 to above 2.6 MHz was achieved when the phosphor was replaced by the QDs [16]. In addition, using digital modulation techniques such as on-off keying (OOK), data rates of up to 280 Mb/s were realized from a micro-LED with perovskite QDs [17].

For most reports on the optical bandwidth of QDs, the solid-state light sources were arranged by spatially separating from the QDs [17, 18] or by QD coating on the LED surface [14]. A longer wavelength signal is generated by a radiative energy transfer process that converts short



wavelength light to long wavelength. The E-O response time is determined by the carrier injection to the LED active region (carrier transit time across the semiconductor and resistance-capacitance (RC) time delay), carrier lifetime before short wavelength photons are generated, and the radiative energy transfer time when the electrons in QDs are excited and converted to long wavelength photons, etc. In addition to the radiative transfer, the energy transfer process can be nonradiative, a so-called Förster resonance energy transfer (FRET). When the QDs are close to the LED active region, electrons can directly transfer to QDs without going through short wavelength photon generation and electron excitation in the QDs. Intuitively such a process is faster than the radiative transfer. The bandwidth thus potentially increases.

FRET has been investigated by embedding QDs in the LED nanostructures. For example, by bringing colloidal nanocrystals (NQDs) to the deep etched patterns in a LED, a twofold enhancement of the colloidal NQD emission is demonstrated and attributed to non-radiative energy transfer [19]. In addition, even though LEDs with photonic crystals (PhCs) have been explored for VLC [20-22], the study of QDs embedded within the nanopatterned LED active region for E-O modulation is rarely studied.


## 1.3 Thesis Outline



The organization of this thesis is as follows:

In chapter 2, the LEDs embedded with PhCs nanohole structure for high-speed data transmission are discussed. LEDs can get better bandwidth by shrinking the mesa area, however this comes at the expense of decreased light output power. Small and large signal modulations were all measured and analyzed in this chapter. Also, OOK modulation was used to examine the capabilities of data transmission. In this case, 400 Mbps eye pattern was seen.

In chapter 3, the LEDs integrated with QDs for high-speed data transmission are also discussed. Electro-optical (E-O) frequency response method was utilized to simply measure the LED's frequency response. After that, the capability of data transmission was also investigated by using OOK modulation. Finally, only the light output of QDs was analyzed in the E-O frequency response.



# **Chapter 2. Background of High-Speed Modulation of Two-dimensional Photonic Crystal GaN LEDs**

## **2.1 Background of Photonic Crystal LEDs**

By applying formulae to Maxwell's equations and the vector Helmholtz equation in 1979, Ohtaka was the first to compute and present the idea of a photon energy band in diffraction as an addition to Mie and Debye theories [23]. In 1987, Yablonovitch [24] and John [25] elucidated the effect of suppressed spontaneous emission in photonic crystal (PhC) heterostructures. As a result of the analogy between PhCs and semiconductors, substantial study was begun shortly following these works. There are features of photonic band gaps PBGs, dispersion relations, and pass bands that allow the PhC heterostructure to be expanded from semiconductors to the optical domain [26]. So, there have been several applications of semiconductor nanofabrication in the field of electro-optics (EO), including high-speed lasers, low loss waveguides, photovoltaic cells, high efficiency LEDs, and add-drop filters. [26, 27].

Due to the photon being released from a material with a high refractive index, the light output power of LEDs is often restricted by the efficiency at which light can be

extracted.  $1/4n^2$  represents the measured light extraction fraction. In the instance of the GaN LED with a value of  $n = 2.5$ , it is only possible to extract 4% of the light from the material, which results in a narrow escape cone with a critical angle of 23.6 degrees due to the total internal refraction (TIR). Therefore, surface roughening methods are frequently utilized to extract guided light in GaN LEDs. Particularly appealing aspects of 2D PhC texturing are the ability to regulate light directionality and excellent extraction efficiency. The Bragg's law of diffraction may be used to describe the light dispersed by PhCs

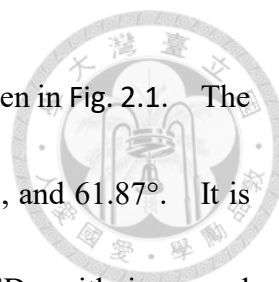
$$\vec{K}_d = \vec{K}_{||m} + p * \vec{G}_0$$

where  $k_d$  represents the in-plane wavevector of the diffracted light,  $k_{||m}$  represents the in-plane wavevector of the incident light,  $p$  represents the harmonic order of diffraction, and  $G_0$  represents the reciprocal lattice vector supported by PhCs [28]. With the change from PhCs, the 1D Helmholtz equation can be used to get the profiles of diffracted modes

$$[\vec{\nabla}^2 + \frac{\omega^2}{c^2} \varepsilon_r(z)] \vec{E}_n = 0$$

where  $\varepsilon_r(z)$  represents the LED's transverse dielectric constant distribution,  $E_n = E_{n,0} e^{i\beta_n r_{||}} E_n(z)$  represents the n-th mode with  $r_{||} = (x, y)$ , and  $E_n(z)$  represents the transverse profile of  $E_n$  [28].

The guided modes turn into leaky modes into the air due to the PhCs' diffraction.



An example of mode extraction using a 450 nm wavelength may be seen in Fig. 2.1. The angles at which three guided modes are extracted are 19.47°, 35.26°, and 61.87°. It is clear that PhCs may greatly improve the performance of PhCLEDs with improved directionality and increased extraction efficiency.

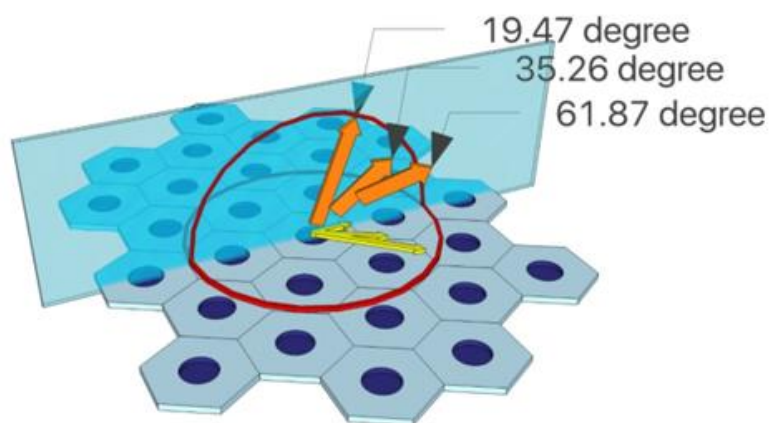


Fig. 2.1 3rd-order  $\Gamma$ M diffraction by PhCs with a 520 nm-period hexagonal lattice.

Three diffraction angles for 450 nm wavelength extracted modes were determined.



## 2.2 Process Flow of Photonic Crystal LEDs

In our work, a GaN buffer layer, a 2- $\mu\text{m}$  Si-doped n-type GaN layer, ten 17-nm-thick InGaN/GaN multiple quantum wells (MQWs) active regions, and a 160-nm Mg-doped p-type GaN layer were grown by metal-organic chemical vapor deposition (MOCVD) on a c-plane sapphire substrate. The wavelength of peak emission is 454 nm, and the electroluminescent spectrum has a full width at half maximum (FWHM) of roughly 45 nm.

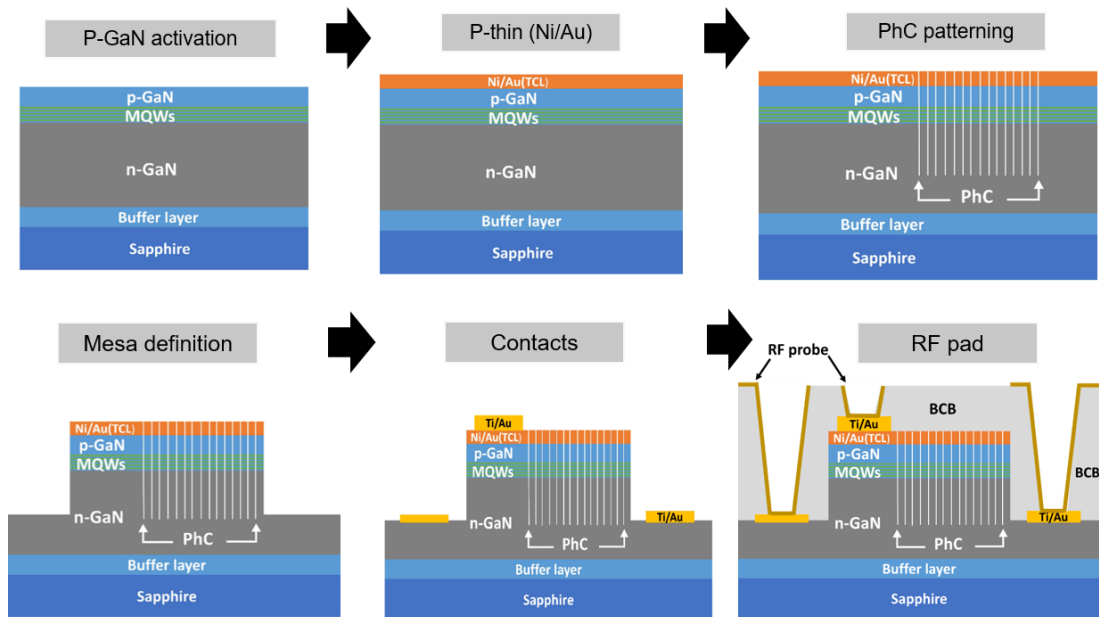


Fig. 2.2 Process Flow of PhCLEDs

The modulation bandwidth of the small signal electro-optical (E-O) response was optimized using the PhC patterns and their accompanying geometrical configurations [21].

Our PhC pattern's scanning electron microscopy (SEM) picture is depicted in Fig.

2.3. The PhC pattern is given with a 500 nm period and a 200 nm nanohole radius. Now, PhC LEDs (PhCLEDs) with mesa dimensions of  $80 \times 80$  and  $120 \times 120 \mu\text{m}^2$  were developed and named as PhC-80 and PhC-120, respectively. We also developed conventional LEDs (CLEDs) using the identical procedure methods, with the exception of PhC pattern design. CLEDs are flattened structures devoid of nanoholes. C-80 and C-120 denote CLEDs with the equivalent mesa sizes, according to the nomenclature of PhCLEDs.

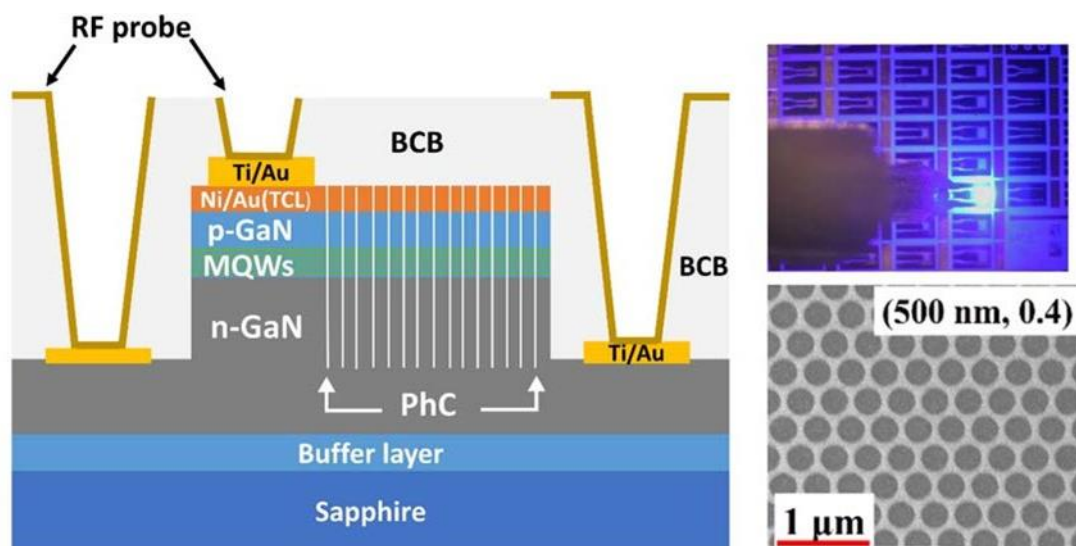


Fig. 2.3 (a) A schematic drawing of a PhCLED's cross-section. (b) The micro picture of a 5mA LED current. (c) SEM photograph of a photonic crystal patterns.



## 2.3 Characteristics of the DC Feature



For PhC-80 and C-80, a 10mA injection current produces peak emission wavelengths of 444.3 nm for C-80 and 445.2 nm for PhC-80 at the injection currents as shown in Fig. 2.4. The emission spectra of PhC-80 and C-80 have virtually identical full-width at half maximum (FWHM) values of 16 nm and 17 nm, respectively. Luminescence-current-voltage (L-I-V) characteristics curves of the devices are depicted in Fig. 2.5. (L-I-V) characteristics curves of the devices are depicted in Fig. 2.4. PhC patterns may aid in LED light extraction, although the optical output power of PhCLEDs is often lower than CLEDs in this investigation. This is due to the PhCLEDs' effective active area having a substantially smaller area with the same mesa size of  $80 \times 80$  and  $120 \times 120 \mu\text{m}^2$ . The size of the mesa is 44% smaller in PhC-80 than in C-80, and it is 34% smaller in PhC-120 than in C-120. The light output power of the PhC-120 and PhC-80 is 67% and 71% lower than the CLEDs with the same mesa area when the injection current is 40 mA, respectively. The output power of CLEDs and PhCLEDs is not directly related to the size of the mesa because of the PhC structure's ability to enhance LED light extraction. Despite their lower light output power, the focus of this research is on the PhCLEDs' capacity to transmit high-speed data rather than their light output power.

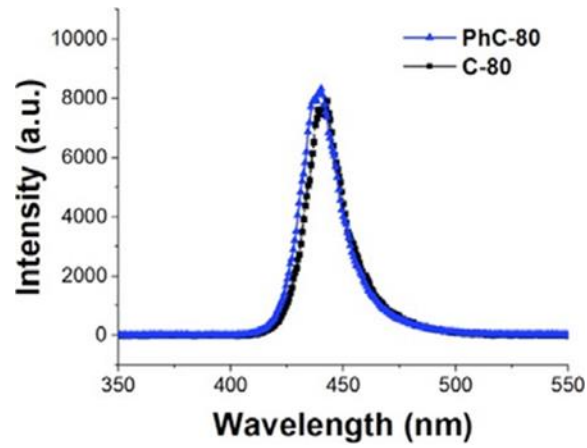


Fig. 2.4 Electroluminescence spectra of PhC-80 and C-80.

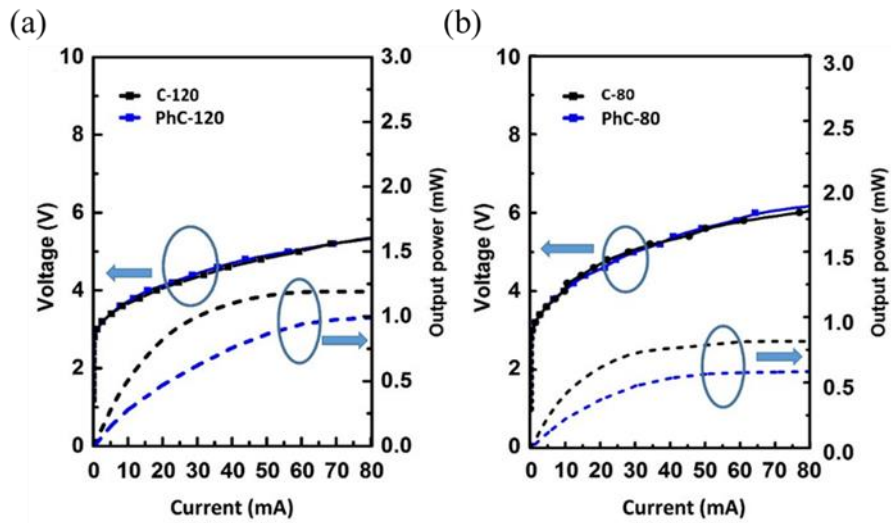
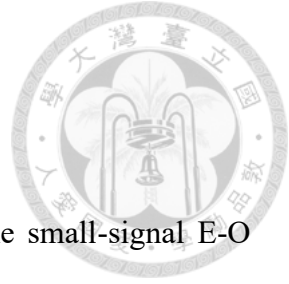


Fig. 2.5 L-I-V curves of (a) PhC-120 and C-120, and (b) PhC-80 and C-80.



## 2.4 Electro-Optical Behavior of PhCLEDs

Using a vector network analyzer (VNA, Agilent N5225A), the small-signal E-O modulation response was extracted in order to confirm the optical frequency response of our LEDs. As shown in Fig. 2.6, this measurement was done using the standard Short, Open, Load, and Thru (SOLT) calibration method, which makes sure that the RF probes and connecting wires are de-embedded of parasitic resistance and capacitance. A bias tee (Anritsu, V225) was used to connect the small electrical signal to a DC source following SOLT calibration. A high-speed silicon photodetector (New Focus, 1601FC-AC) was used to analyze the optical response after the light output of the LED was gathered using an optical fiber. The vector network analyzer (VNA) was used to analyze the electrical signal from the photodetector (PD). The frequency at which the magnitude of optical output power drops to half its DC value is defined as the RF bandwidth.

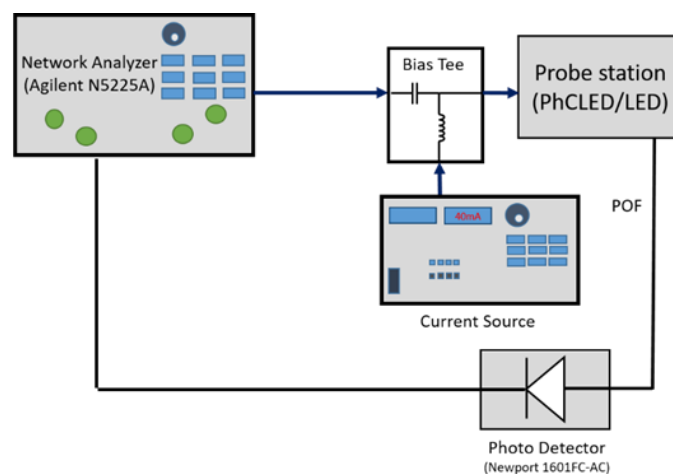


Fig. 2.6 Experimental configuration of the frequency response system.

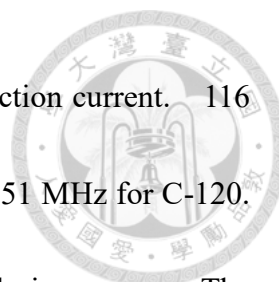
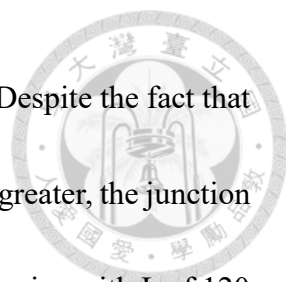


Fig. 2.7 depicts the optical frequency responses at a 40mA injection current. 116 MHz is the -3dB modulation bandwidth for PhC-120, as opposed to 51 MHz for C-120. As we decrease the size of the mesa, the frequency bandwidth increases. The modulation bandwidth of PhC-80 is 178 MHz, while that of C-80 is only 83 MHz. To minimize RC delay, a smaller light-emitting mesa can be used to increase small signal E-O frequency response [29]. To maintain an acceptable signal-to-noise ratio (SNR), however, adequate light output power is required. The PhC-80 and C-80 will also be employed for further large signal analysis, as will be discussed later.

The enhanced radiative recombination rate and shorter spontaneous radiative lifetime are primarily responsible for the better E-O frequency response of PhCLEDs. The increased modulation bandwidth of LEDs with PhC nanoholes is mostly due to the faster photon decay rate, photonic model extraction, and therefore shorter radiative recombination lifetime [21, 29]. Along with improving internal quantum efficiency (IQE) with strain relaxation, the nanohole structure also increases the probability of photonic modes scattering [21]. The contents of the talks on the relation between the effective carrier radiative lifetime and RC-limit of our devices have been described in our prior work [29]. Fig. 2.8 depicts the extracted parameters and the small-signal circuit model. The measured  $S_{11}$  of  $2 \times 2$   $S$ -parameters from the devices was fitted to extract the intrinsic components, which included contact inductance ( $L_s$ ), contact resistance ( $R_{s2}$ ),



junction diffusion capacitance ( $C_d$ ), and junction conductance ( $g_j$ ). Despite the fact that the junction conductance and contact resistance of a smaller mesa are greater, the junction capacitance of the device with  $L$  of  $20\ \mu\text{m}$  is only 4% of that of the device with  $L$  of  $120\ \mu\text{m}$ , for both CLEDs and PhCLEDs. Same-sized PhCLEDs and CLEDs have a comparable intrinsic RC time constant ( $\tau_{RC} = R_{s2}C_d / (R_{s2}g_j + 1)$ ). As a result, the increased E-O bandwidth of PhCLEDs over CLEDs is related with a shorter spontaneous radiative recombination lifetime rather than the size-induced impact.

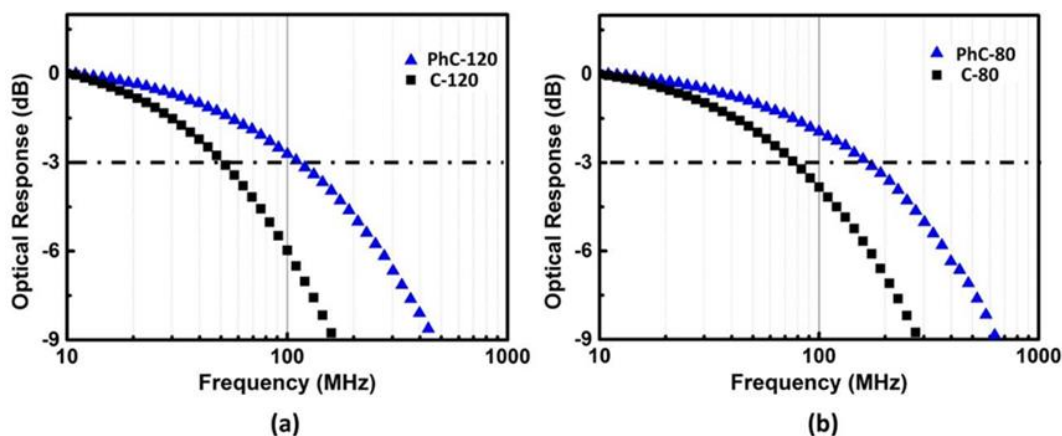


Fig. 2.7 Optical frequency responses of CLEDs and PhCLEDs with the mesa size of (a)  $120 \times 120\ \mu\text{m}^2$  (b)  $80 \times 80\ \mu\text{m}^2$  under 40mA current injection.

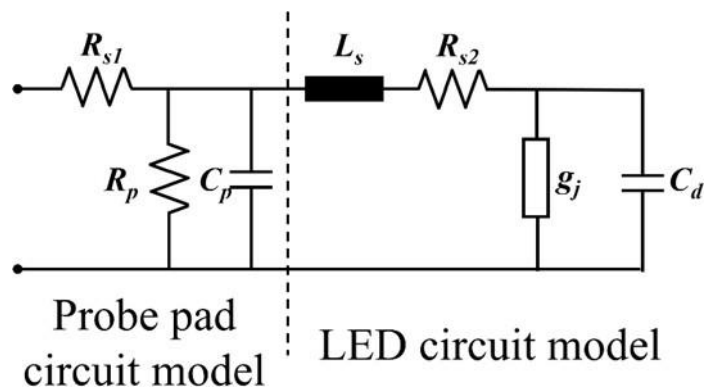


Fig. 2.8 Small-signal equivalent model of LEDs with RF probe pads.



## 2.5 On-off Keying (OOK) Technique

In VLC system, the optical signal is collected quickly by a photon detector because data is superimposed directly onto the modulation of light intensity of an LED. OOK modulation was utilized because of its easy implementation while yet retaining a high-speed performance. This was done so that the data transmission capacity of LEDs could be shown. In the non-return-to-zero OOK (NRZ-OOK) concept (see Fig. 2.9 (a)), the existence of a carrier for a certain time indicates a binary one, whereas its absence for the same period indicates a binary zero [30]. The OOK modulation strategy was employed in this study to evaluate LEDs' capacity to modulate large signals. Fig. 2.9 (b) shows the eye diagram for evaluating the application in VLC connections.

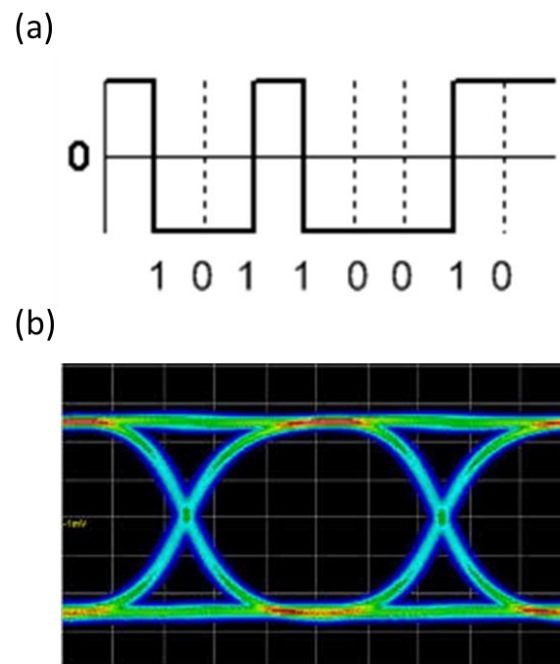
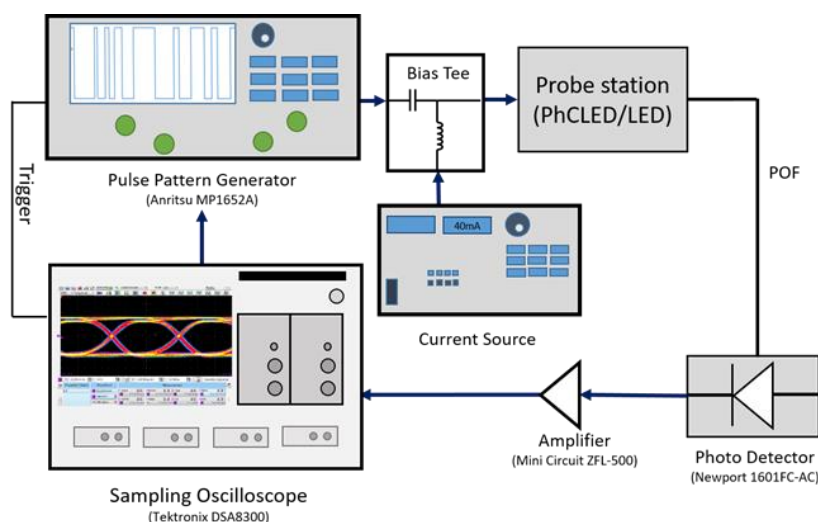


Fig. 2.9 (a) A non-return-to-zero binary code (b) The eye diagram pattern



## 2.6 PhCLEds with Digital Modulation

On-off-keying (OOK) modulation was used to investigate the PhCLEds and CLEDs' large signal responses. A pulse pattern generator (PPG) creates a  $2^7-1$  bit length pseudo-random bit sequence (PRBS) for OOK modulation, which uses a none-return-to-zero (NRZ) data pattern. With a bias tee (Picosecond PSPL5545), an RF signal was added to a DC biasing current and then applied to devices. A 1 GHz high-speed photodetector was used to detect the modulated E-O signal after it had been captured by an optical fiber probe. Before the electrical data from the photodetector was entered into the oscilloscope (Tektronix DSA8300), it was made 42 dB stronger with the help of a broadband amplifier (Mini Circuit ZFL-500). Fig. 2.10 was a schematic depiction of the measurement setup. To keep high-speed performance from being affected by heat, LED chips were put on a probe station where the temperature was kept constant at 24°C.



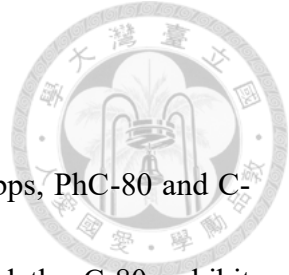


Fig. 2.10 Setup for measuring of the OOK modulation system.

According to their different data rates of 100, 200, and 400 Mbps, PhC-80 and C-80's eye diagrams are shown in Fig. 2.11. Both the PhC-80 and the C-80 exhibit extremely clear eye opening at 100 Mbps, demonstrating that two types of LEDs are suitable for VLC applications at this data rate. Normally, with an increase in data rate from 100 to 400 Mbps, the eye patterns gradually worsen. Comparing the SNR of PhC-80 and C-80 at various bit rates is depicted in Fig. 2.12. The SNR declines as the data rate increases, according to the curve trend. In general, greater SNR performance would result from higher optical power. Since the optical light output of CLEDs is 40% more than that of PhCLEDs at data transmission speeds below 300MHz, C-80 has a better SNR. But when the data rate goes over 300Mbps, the CLEDs' modulation bandwidth goes down. This means that the E-O modulation response can't keep its signal level at a high modulation rate, which causes the SNR to go down. In this situation, the device's modulation bandwidth wins out, improving the SNR of PhC-80 at 400Mbps. Fig. 2.13 shows the bit-error-rates (BERs) for different received optical powers at 200 Mbps and 400 Mbps data rates. PhC-80 has smaller BER curves than C-80 in both situations. It shows that PhCLEDs are better suited for high-speed data transmission.



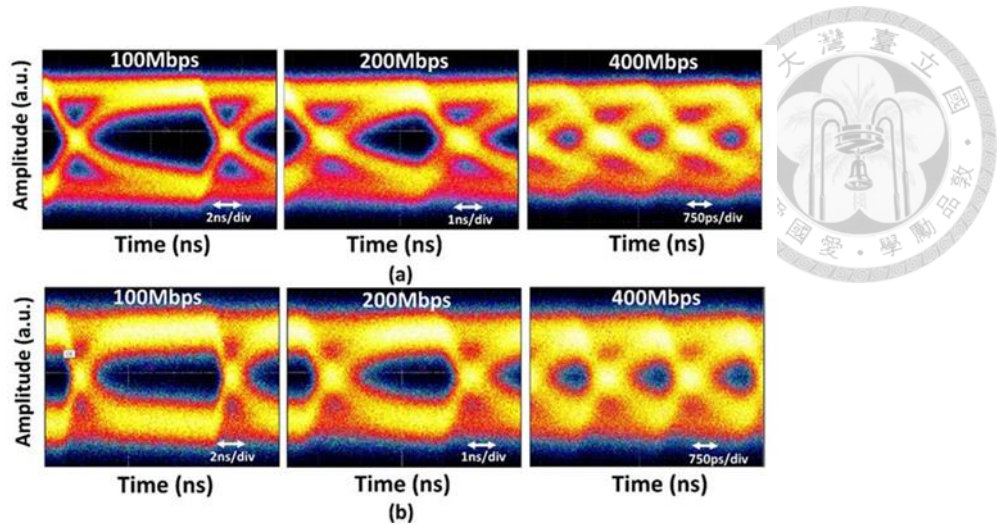


Fig. 2.11 Eye diagrams of (a) C-80 and (b) PhC-80 at data rates of 100Mbps, 200Mbps, and 400Mbps.

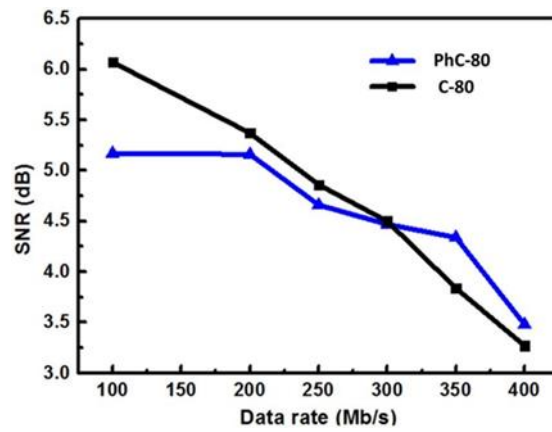


Fig. 2.12 SNR performance of the PhC-80 and C-80 at various transmission data rates.

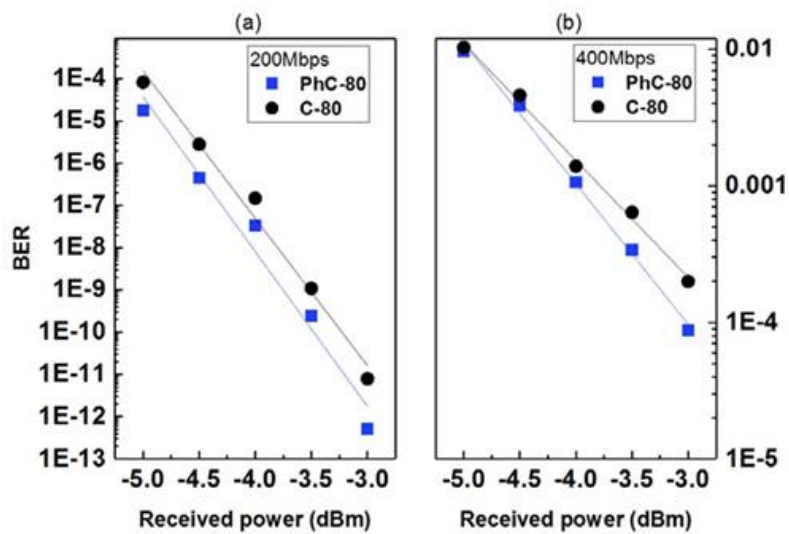
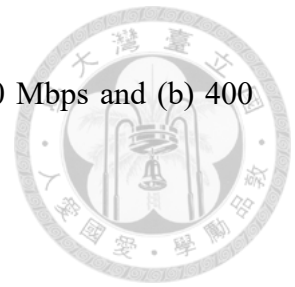


Fig. 2.13 BER curves for PhC-80 and C-80 at data rates of (a) 200 Mbps and (b) 400

Mbps.



## 2.7 Summary



In this part, we analyzed PhCLEDs and CLEDs, which utilize OOK modulation to demonstrate data transmission. Both PhCLEDs and CLEDs exhibit an open-eye pattern at transmission rates of up to 400 Mbps in the OOK data transmission experiment, suggesting that high-speed transmission is possible. Due to their greater DC light output power than PhCLEDs, CLEDs have better SNR at low frequencies; however, PhCLEDs have higher SNR at frequencies over 300 MHz. It means that the high frequency performance is dominated by the optical response bandwidth.

# Chapter 3. Quantum Dots Integrated with Photonics Crystal LED for Visible Light Communication



## 3.1 Background of Quantum Dots

Substances are becoming increasingly minuscule as technology advances. The chip size is lowered in order to accommodate more functionalities in a given area in the technology business. Nanotechnology even has increasingly become a goal of worldwide interest, whether it is in technology or the medical business.

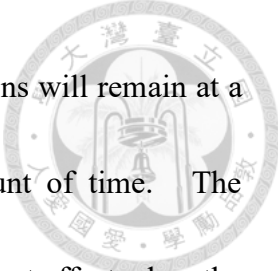
The architectures of semiconductors can be categorized according to their dimensions at the quantum scale as follows: three-dimensional materials, two-dimensional quantum wells, one-dimensional quantum wires, and zero-dimensional quantum dots (QDs). The density of states tends to grow more discontinuous if there is a rise in the dimension of the confined carrier. Four groups of nanomaterials may be distinguished: those based on inorganic, carbon, organic and composite substances [31]. In the last several years, QDs have gotten a great deal of interest as a potential new generation of luminous materials.

## 3.2 Colloidal Quantum Dots



Colloidal quantum dots (QDs), which are organic semiconductor nanocrystals, have exhibited color purity, high photoluminescence, and tunability of wavelength based on size in solid-state lighting (SSL) applications and thin film display [32]. Their electrical and optical characteristics may be altered by adjusting their sizes, forms, and chemical composition [33]. Crystals made of colloidal quantum dots generally have a radius of between 2 and 10 nm. Specifically, as nanocrystals, QDs are capable of confining excitons in small, dispersed recombination channels and inconsistent energy band gap because of quantum confinement effects [34]. The emission wavelength is determined by the quantum confinement effect, which is dependent on the colloidal quantum dots' size. The size of QDs may be altered by changing the emission wavelength; small QDs have a shorter emission wavelength, whereas large QDs have a longer emission wavelength.

Solid QDs, such as CdSe, which have been dissolved in an organic solvent to form colloidal quantum dots (e.g., toluene). This substance is made through the process of chemical synthesis. The reagent is first placed inside the bottle, and then the container is heated to enable the chemical reaction, breakdown the reactant, and finally produce the quantum dots.



Excitation of a quantum dot produces an exciton, and the excitons will remain at a particular distance, known as the Bohr radius, for a certain amount of time. The excitonic transition energies go up because of the quantum confinement effect when the size of the particle gets close to the Bohr radius. Excitons are only able to be contained within a restricted distance due to the fact that the radius of QD is shorter than the Bohr radius (generally smaller than 10 nm). Due to the Pauli Exclusion Principle stating that no two electrons and holes can share the precise identical energy level, a quantum confinement effect will occur when holes and electrons are compressed into a dimension that is nearing the critical point.

To sum up, QDs are schematically depicted in Figure 2.2 as having an inorganic semiconductor core (2–10 nm in diameter), an inorganic semiconductor shell (which is broader), and an organic ligand coating (which serves to passivate the inorganic semiconductor shell). In addition, Surface passivation and a three-dimensional confinement of excitons and oxygen in Colloidal QDs increases photo-stability [35]. As a result, QDs have the potential to be used in optoelectronics and color-converted materials because of their tunable band gap and high quantum yield [36].

### 3.3 Förster Resonance Energy Transfer



Förster resonance energy transfer (FRET) is a process that describes how light-sensitive molecules exchange energy. Non-radiative transfer through dipole-dipole coupling may allow an excited donor to transmit energy to an acceptor [37]. This energy transfer efficiency is inversely proportional to the distance between the donor and acceptor to the sixth power, which makes FRET particularly sensitive to small distance changes. The most common method by which blue light can excite quantum dots is as follows: when blue light emits photons as a result of radiative recombination, the quantum dots absorb the photons for the purpose of energy transfer. This causes the quantum dots' internal excitons to recombine, which in turn causes the emission of light from the quantum dots. When it comes to FRET, however, there is no photon absorption or emission since the energy is transferred from an excited-state molecule (donor) to a lower-state molecule (acceptor).

The process of FRET is related to that of near-field transfer in the sense that the reaction may be carried out over a distance that is significantly less than the wavelength of the light source [38]. In the area of the electromagnetic spectrum known as the near-field, the excited state of the donor chromophore is responsible for emitting virtual photons, which are then promptly taken in by the acceptor chromophore. It is

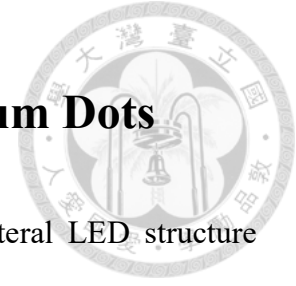
impossible to detect these photons since their very existence goes against the principles of energy and momentum conservation. As a result, the process of FRET is seen as one that does not involve the radiation process.



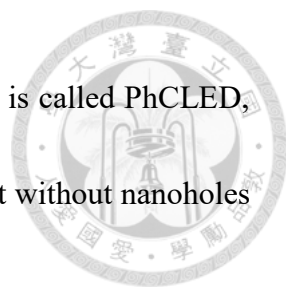
Life time measurement is a potential tool for measuring quite a transfer process. The degree to which the fluorescence lifetime of the donor has changed can be used to determine FRET efficiency. When the acceptor exists, the donor's life time will shorten. So, time-resolved photoluminescence was utilized for the purpose of determining the FRET lifetime measurement [39]. The FRET efficiency is dependent on several physical characteristics, including the distance between the acceptor and the donor and the overlap between the absorption spectrum of the acceptor and the emission spectrum of the donor. In our research, we came up with a new way to make the distance between the donor and the acceptor shorter, and we put it into the structure of the LED. Quantum dots are usually made on the surface of the light-emitting element. However, our idea can reduce the distance between the quantum dot and the quantum well (QW), which will make the FRET process work better.



### 3.4 Process Flow of PhCLEDs with Quantum Dots



The light-emitting device in this study is composed of a lateral LED structure embedded with photonic crystal (PhC) nanohole patterns and green colloidal quantum dots. For green colloidal quantum dots will discuss later. First, on top of the sapphire substrate, a 104.1nm Mg-doped p-type GaN layer, ten periods of InGaN/GaN MQW active region, and a 2- $\mu$ m Si-doped n-type GaN, and a GaN buffer layer were grown by metal-organic chemical vapor deposition (MOCVD). The process starts from depositing Ni/Au (5nm/5nm) thin layers by electron-beam evaporation. A silicon nitride (SiN) was deposited on the surface of the structure as a mask before electron beam lithographing. The photonic crystal nanohole patterns was defined by electron beam lithography followed by inductively coupled plasma reactive ion etching (ICP-RIE). The depth of PhC holes is around 600 nm. A top view of the PhC patterns on the LED mesa is shown in Fig. 3.2. The period and radius of the nanohole in our design are 500 and 200 nm, respectively. Next, a 120x120 $\mu$ m<sup>2</sup> mesa was then also etched by ICP-RIE with a depth of 600nm in Fig. 3.1(c). As shown in Fig. 3.1(d), the n-type contact metal, Ti/Au/Ni/Au (250/1250/500/1250 nm), was evaporated. The device was then sealed by Su-8 polymer. An interconnect contact probe pad, Ti/Au (50/1300 nm), was deposited after the VIAs was opened. Shown in Fig. 3.1(g) is the lateral profile of the device for



VLC characterizations. In this work, the LED with PhC nanoholes is called PhCLED, while the conventional LED of the same  $120 \times 120 \mu\text{m}^2$  mesa size but without nanoholes is called CLED.

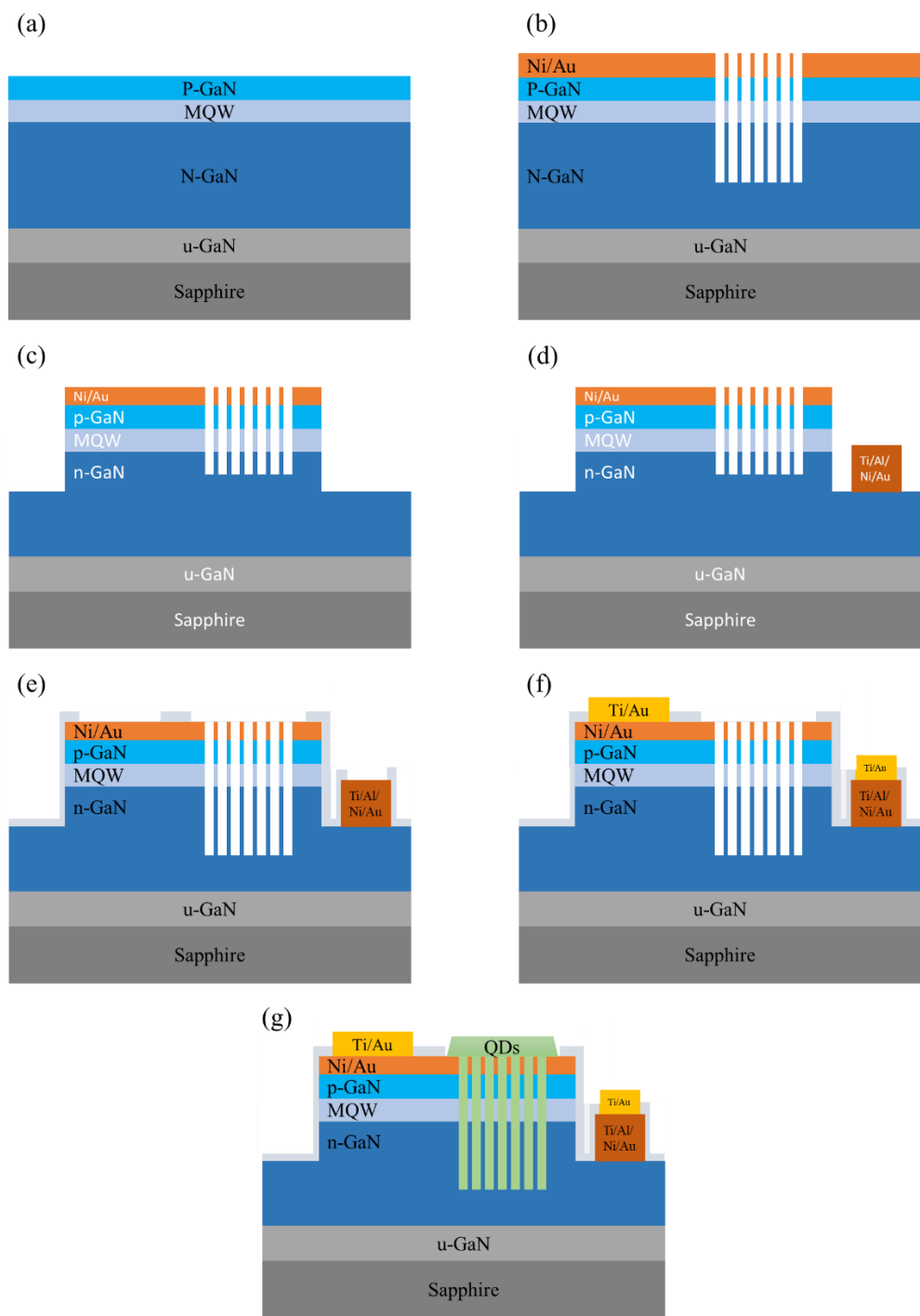


Fig. 3.1 Process flow of lateral PhCLED

Before device measurement, green colloidal CdSe QDs were pre-mixed in toluene before spraying on the light-emitting area by the aerosol jet (AJ) printing technique. Three different QD layer thicknesses were chosen for studying light transmission behaviors. Because it's not easy to quantify the exact amount of QDs on the LEDs, the effect of QDs on the optical behaviors is benchmarked by the amount of color conversion from blue to green. And the nomenclature of the conventional LED (CLED) with a QD spray time of 300, 400 and 500 ms is QD-CLED-A, QD-CLED-B and QD-CLED-C, respectively. We also prepare a PhCLED with QD coating time of 300 ms, which is named QD-PhCLED in this work. The device profiles of QD-PhCLED and QD-CLED are shown in Fig. 3.3.

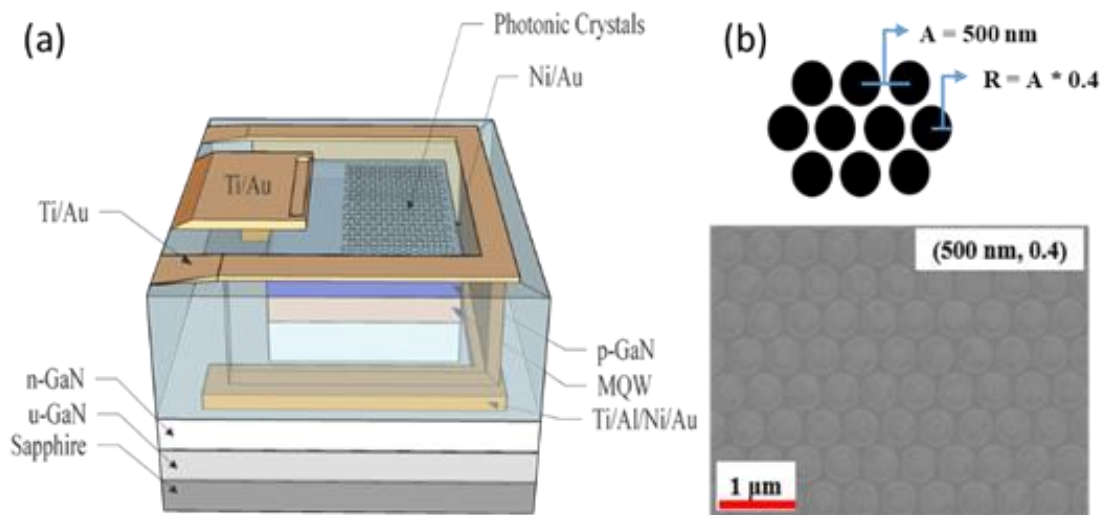


Fig. 3.2 (a) Schematic and structure of the PhCLED. (b) SEM image of the PhCs nanohole arrays.

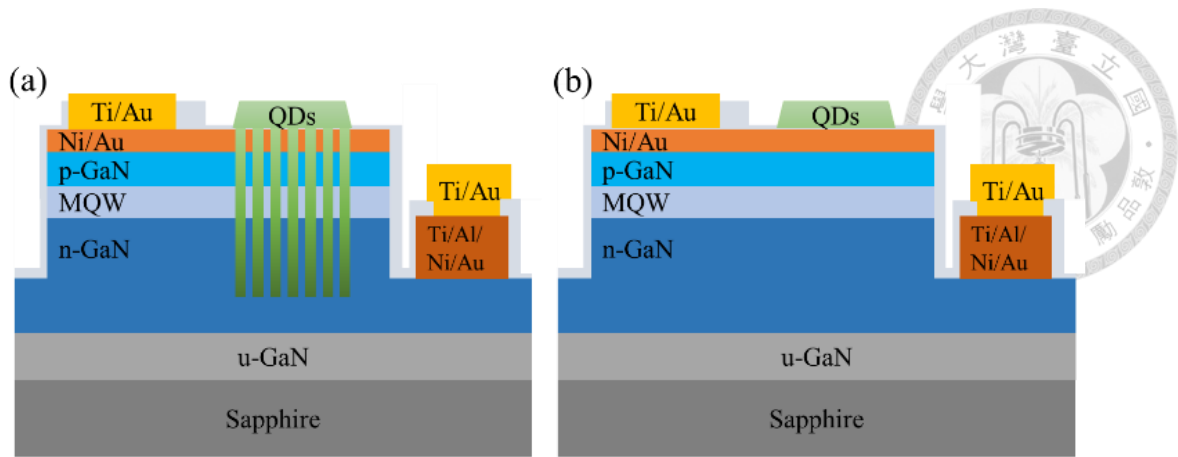


Fig. 3.3 Schematic diagram of (a) QD-PhCLED, (b) QD-CLED. In this work, QD-CLEDs have three different QD coating thicknesses.

### 3.5 Characteristics of the DC Feature of Conventional LEDs and PhCLEDs



The electrical characteristics of PhCLED and CLED were measured by the HP 4155C semiconductor parameter analyzer. The luminescence-current-voltage (L-I-V) curves are shown in Fig. 3.4, and the forward current level of PhCLED is slightly lower than that of CLED because the nanohole patterns increase the overall contact resistance and internal resistance. Though nanoholes help to increase external light extraction, the light output intensity of the PhCLED is lower than that of CLED because of the decreased light-emitting area with the existence of nanoholes. At an injection current of 5mA, light output of PhCLED and CLED is 227.9 and 287.9 $\mu$ W, respectively, indicating a 21% loss of output power for a PhCLED as compared to a CLED. Despite the nanohole patterns help to increase external light extraction [20, 29], the light output intensity of the PhCLED is lower than that of CLED because the nanoholes sacrifice the light emitting area. In this work, we focus on the capability of data transmission and modulation in frequency domain. The amount of light output power isn't the main concern.

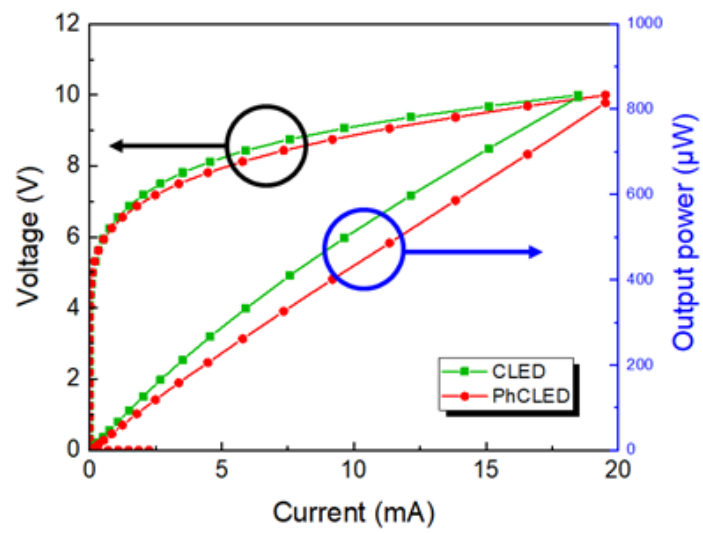


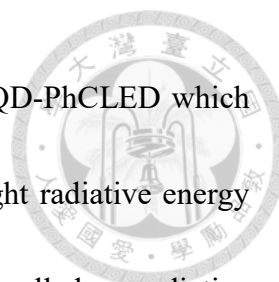
Fig. 3.4 L-I-V curves of PhCLED and CLED.

### 3.6 Emission Spectra of LEDs with QDs



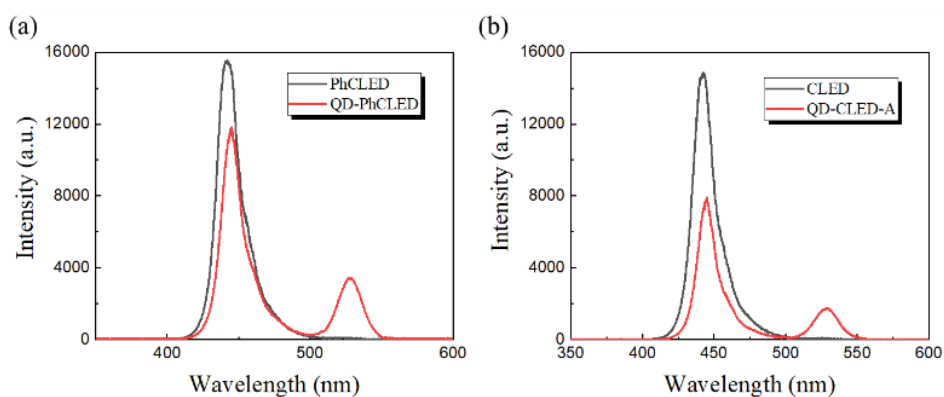
We next characterize light output spectra of the devices using a spectrometer (Ocean Optics, HR 4000). At a bias current of 5 mA, as shown in Fig. 3.5, an emission peak at the wavelength of 441.5 and 442.5 is observed for a PhCLED and a CLED. The colloidal QD coating results in a wavelength conversion from blue to green color. For QD-PhCLED, the QD coating results in a red-shift of blue light from 441.5 to 443.9nm, and a fluorescent green light emission from QDs at 527.2nm (see Fig. 3.5(a)). While for QD-CLED, a red shift of blue light from 442.5 to 445.1 nm and green light at 527.1nm is generated (see Fig. 3.5(b)). The blue to green intensity conversion is demonstrated from the spectra of the devices in Fig. 3.5(c) by normalizing the blue light output in the optical spectra to 1.

To benchmark the dependence of color conversion on the device structure, conversion efficiency (CE), defined as the ratio of green light intensity increase to the blue intensity decrease at each color's peak wavelength, of the devices is plotted in Fig. 3.5(d). The CE of the QD-PhCLED, QD-CLED-A, QD-CLED-B and QD-CLED-C is 50.0, 23.1, 22.5 and 22.1%, respectively. For a QD-CLED, the CE slightly decreases with the increase of QD spraying time because of non-radiative absorption increases with the QD layer thickness. Furthermore, a distinct difference can be observed from a much



higher CE of the QD-PhCLED than those of QD-CLEDs. For a QD-PhCLED which QDs are embedded adjacent to the QWs, in addition to the blue light radiative energy transfer, electrons can be directly transferred from QWs to QDs, a so-called nonradiative energy transfer (see Fig. 3.6). The multi-path energy transfer from QWs to QDs thus increases CE for a QD-PhCLED.

The above phenomenon is illustrated in Fig. 3.6. The FRET process between QDs in PhC nanoholes and QWs is indicated by the red arrows, while the blue light excited (radiative) process is shown in black arrows. The former is considered as a direct green light emission process while the later as a two-step, electron-hole generated blue and blue to green conversion, process. As a result, the conversion efficiency of QD-PhCLED is higher than that of the QD-CLED.





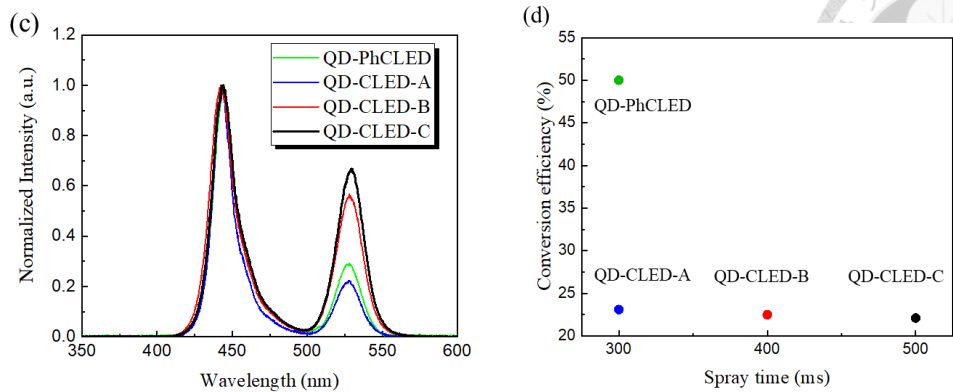


Fig. 3.5 Output spectra of (a) PhCLEDs with and without QDs, (b) CLED and QC-CLED-A. (c) Normalized output spectra of CLEDs with different QDs thickness. (d) Comparison of green to blue light ratio. The blue light output intensity is normalized to 1 for comparisons

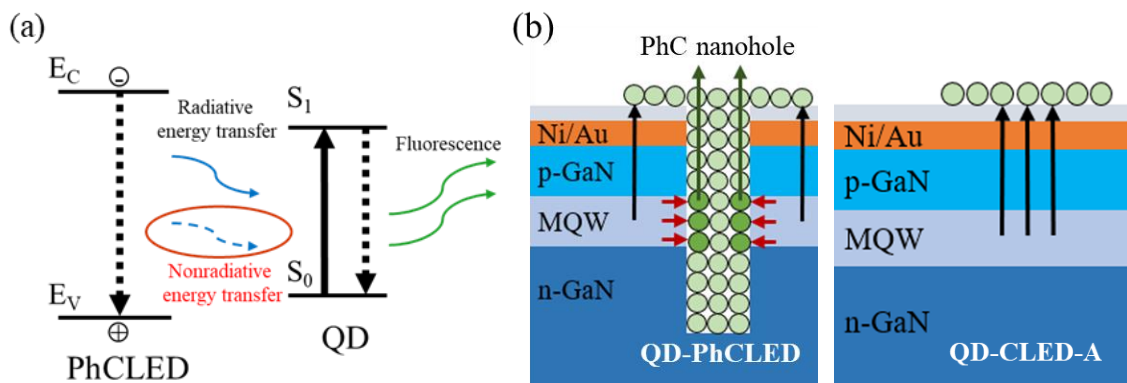


Fig. 3.6 (a) Illustration of the FRET process between the MQW in the PhCLED and QD. (b) Energy transfer paths for the QD-PhCLED and QD-CLED.

Furthermore, from Fig. 3.5(c), it's also noted that the green emission (around 530 nm) underwent a bathochromic shift with the addition of colloidal QDs, as seen in the normalized green light intensity in Fig. 3.7, which is associated with the aggregation and

reabsorption of QD nanoparticles [40]. The combined effect of FRET and photon reabsorption results in the red shift when the amount of QDs is increased for conversion.

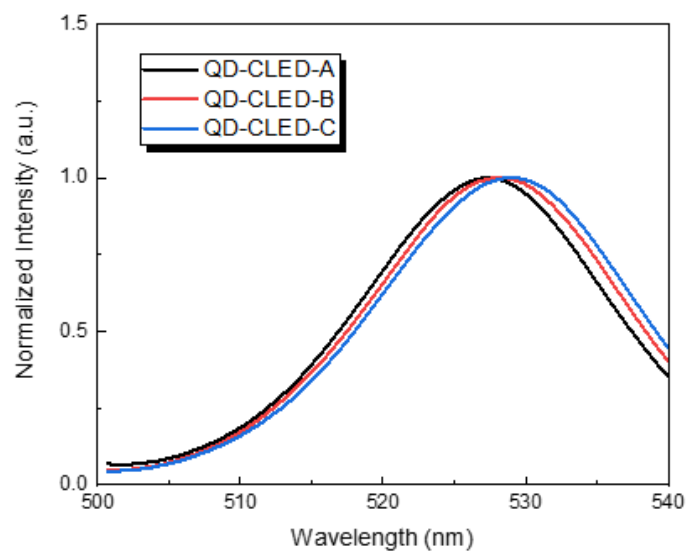


Fig. 3.7 Enlargement and normalization of the green light emission peak in Fig. 3.5.

### 3.7 Electro-to-optical Response Performance



We next conduct an electro-optical (E-O) response measurement of the blue LED with the QDs excited green light. The electrical characteristics of PhCLED and CLED were measured by the HP 4155C semiconductor parameter analyzer. As for extracting E-O (electro-optical) conversion frequency response, the measurement setup is shown in Fig. 3.8. A radio frequency (RF) signal generated from a pulse pattern generator was superimposed with a DC bias through a wideband bias tee. After collecting light output from the LED through an optical fiber, a high-speed silicon photodetector (New Focus, 1601FC-AC) was used to measure the optical response.

The frequency responses under the injection current of 10 mA are shown in Fig. 3.9. The  $-3$  dB conversion bandwidth is 136, 116, 113 and 110 MHz, respectively for QD-PhCLED, QD-CLED-A, QD-CLED-B and QD-CLED-C. First of all, giving the same mesa size of  $120 \times 120 \mu\text{m}^2$  and the same RC (resistance-capacitance) delay time for CLEDs, the decreased  $-3$  dB bandwidth with increasing QDs layer thickness is attributed to the proportion of green light in the detected optical signal. A higher blue to green light output ratio suggests a relative higher blue light output giving the same current injection density and a higher total light output power with both blue and green light contribution. Furthermore, in Fig. 3.9, when the effect of PhC is considered, QD-

PhCLED possesses the highest bandwidth. Since QDs are in close contact with the MQWs in the nanoholes, carriers in QWs are transferred directly to QDs through nonradiative process, which is more efficient in the subsequent green light generation.

A higher -3dB frequency response is thus expected due to the direct carrier transport to the higher energy level of QDs.

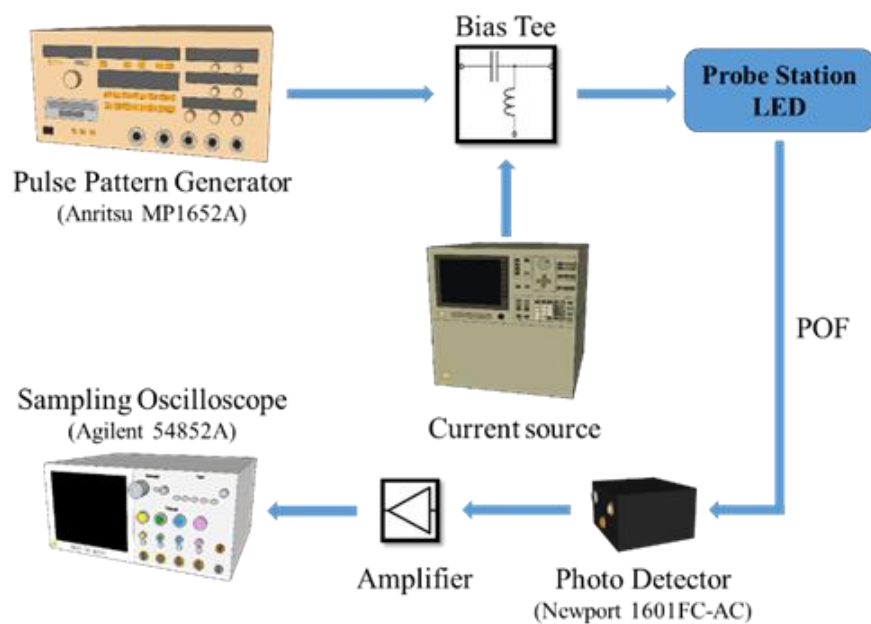


Fig. 3.8 Setup for frequency response system.

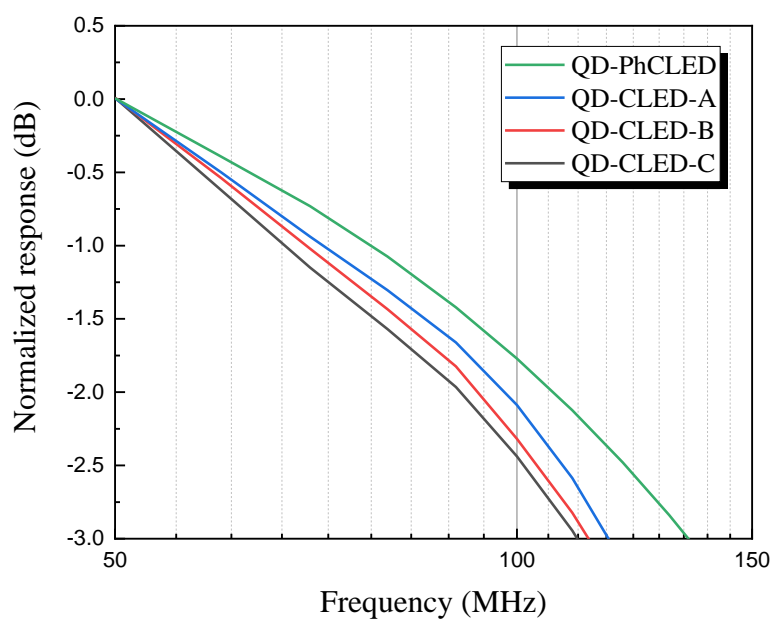
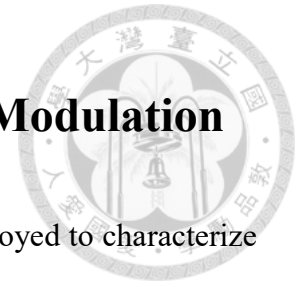
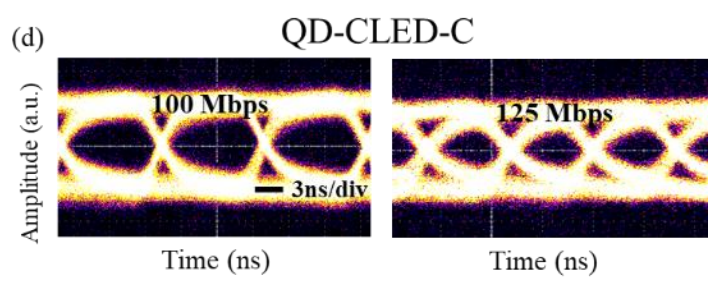
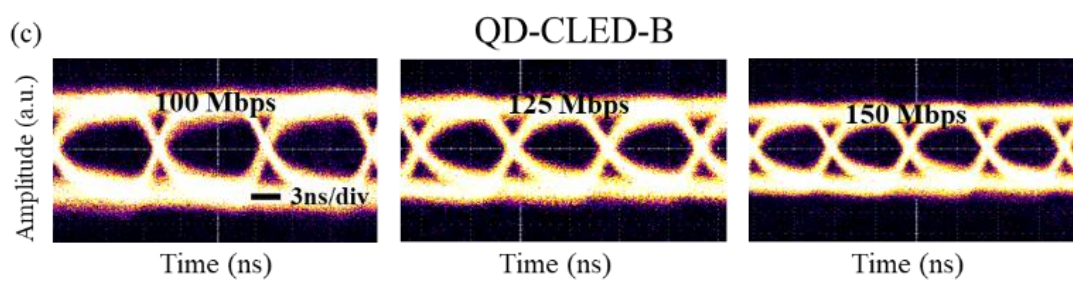
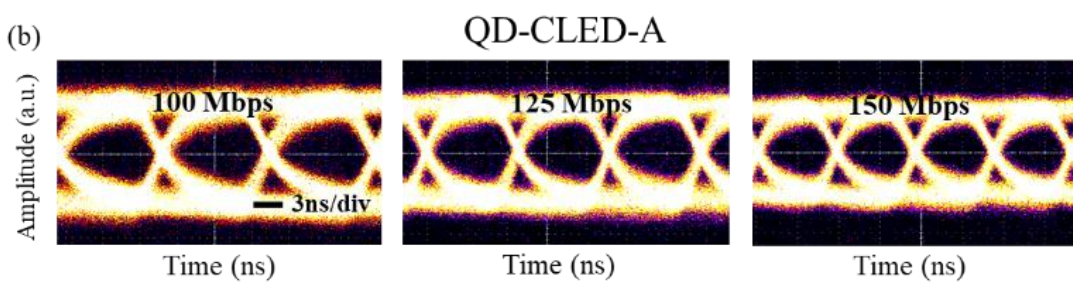
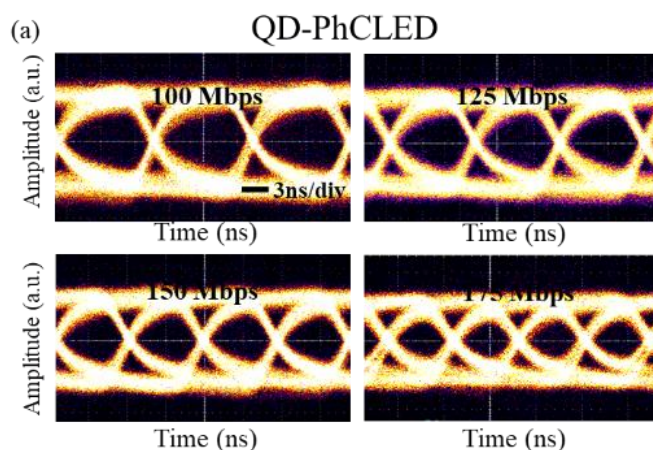
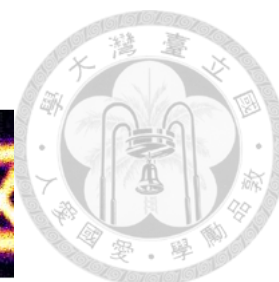


Fig. 3.9 Comparison of frequency responses between QD-PhC-LED and QD-CLEDs.

### 3.8 LEDs Integrated with QDs for Digital Modulation



The non-return-to-zero OOK (NRZ-OOK) technique was employed to characterize the capability of large-signal modulation. Fig. 3.10 shows the eye diagrams of a QD-PhCLED and three types of QD-CLEDs at 100, 125, 150 and 175 Mbps. Due to the equipment limit, eye diagrams with the SNR (signal-to-noise ratio) smaller than 1 are not shown here. Even though all the devices are suitable for VLC applications at the data rate up to 100 Mbps, the performance of eye patterns degrades at a higher data rate. Fig. 3.10(e) shows the corresponding SNRs of the devices at various data rates. The results are correlated to the E-O responses in Fig. 3.9, in which the QD-PhCLED has the best SNR performance. As for QD-CLEDs with various QD spraying times, a thin QD coating and thus a lower blue to green light conversion ratio suggests a stronger overall light intensity. We can thus obtain a higher SNR ratio at a giving data rate operation for QD-CLED-A. The influence of QD coating on the frequency response is very significant, for QD-CLED-C with CE slightly lower than the rest two CLEDs, the eye diagrams can only be benchmarked at data rates of 125 Mbps, beyond which at 150 and 175 MHz, the SNRs are smaller than 1.



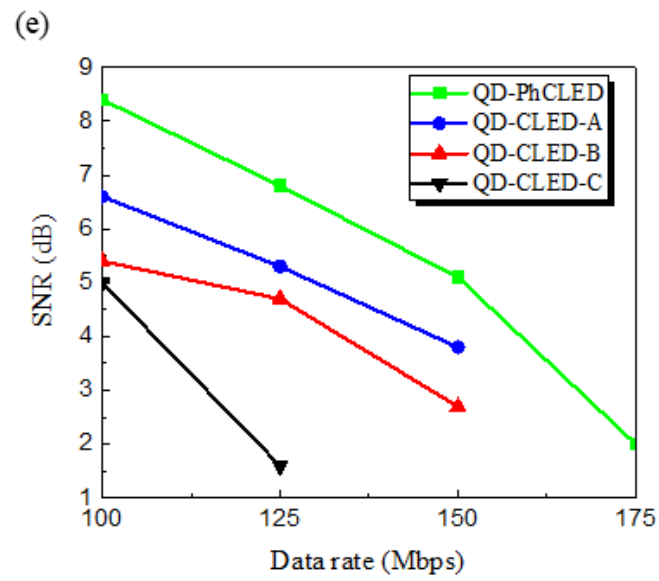


Fig. 3.10 The evaluated eye diagrams of (a) QD-PhCLED, (b) QD-CLED-A, (c) QD-CLED-B and (d) QD-CLED-C. (e) The SNR performance of devices at different data rates.



### 3.9 E-O Response Performance of LED Integrated with only Green QDs



The frequency response and OOK measurements discussed above were performed from the light sources with both blue and green light illuminated from the devices. In this session, we explore the data transmission behavior of only the QD converted green light. A green filter was placed on top of the device to remove the blue light. The E-O frequency response is showing in Fig. 3.11, which suggests -3 dB bandwidth of 81, 83, 78 and 76 MHz, respectively, for QD-PhCLED, QD-CLED-A, QD-CLED-B and QD-CLED-C. Contrary to the E-O response in Fig. 3.9, the -3 dB bandwidth of QD-PhCLED in Fig. 3.11 with only green light is slightly lower than that of QD-CLED-A. The results are mainly attributed to the FRET effect and various distances between QDs and blue light generated MQW active region. First, in addition to transferring blue light to QDs through radiative energy, carriers can also transfer energy from QWs to QDs through nonradiative process for the QD-PhCLED. Second, for QD-PhCLED, QDs are distributed in various distances from the MQWs, as compared with nearly equal distance for QD-CLED-A (see Fig. 3.11(b)). The above two mechanisms suggest green light at different locations is excited at different time giving an electrical signal input, thus creating phase delay of the output green signals for QD-PhCLED. A smaller -3 dB

bandwidth of QD-PhCLED is observed.

To verify the above explanation, time-resolved photoluminescence (TRPL) was next carried out. The devices were photo excited by a 405-nm wavelength laser at an 8 MHz repetition rate. As shown in Fig. 3.12(a), QD-CLED-A (blue line) possesses the shortest carrier life time of 3.188 ns, while QD-PhCLED (green line) has a slightly longer lifetime of 3.440 ns. The results again imply two processes are involved in the green light emission for QD-PhCLEDs. A longer carrier lifetime is thus observed [41, 42].

As for the devices with a thicker QD coating, the E-O conversion is limited by the re-absorption of the green light. The re-absorption process is schematically illustrated in Fig. 3.12(b). Since there are variations of QD diameter in the solution, shorter wavelength photons generated from a smaller QD will be re-absorbed by the QDs with a larger diameter (with a smaller bandgap), generating a longer wavelength (red-shift). The multiple conversion process increases the carrier lifetime. Another factor that influences the carrier lifetime is a thicker QD layer tends to have more QDs aggregated, increasing the chances of multiple re-absorptions. The above mechanisms were validated from the TRPL measurement in Fig. 3.11 and Fig. 3.12, which QD-CLED-C has the lowest  $-3$  dB bandwidth and longest carrier lifetime.

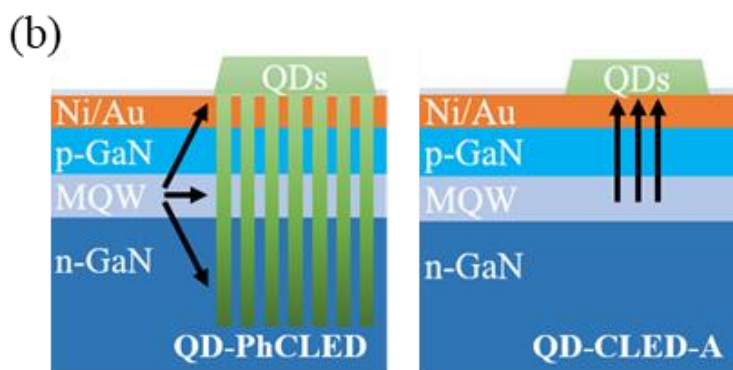
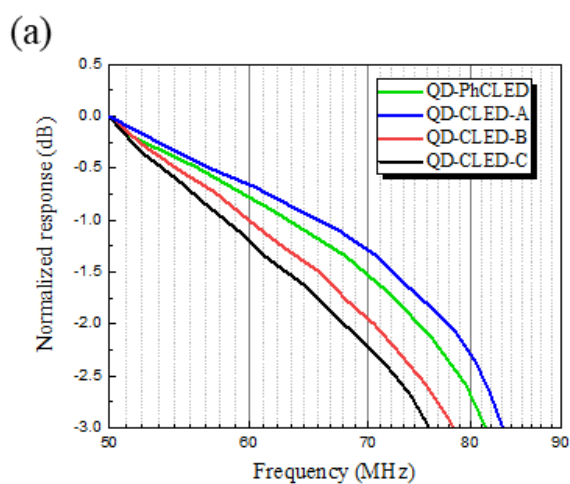
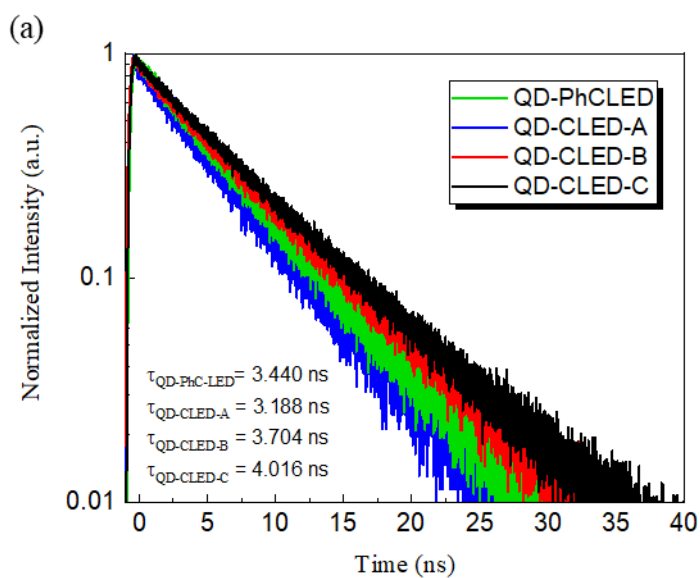


Fig. 3.11 (a) Comparison of frequency responses between only QDs excited green light in QD-PhCLED and QD-CLEDs. (b) Schematic of energy transfer path between QD-PhCLED and QD-CLED.



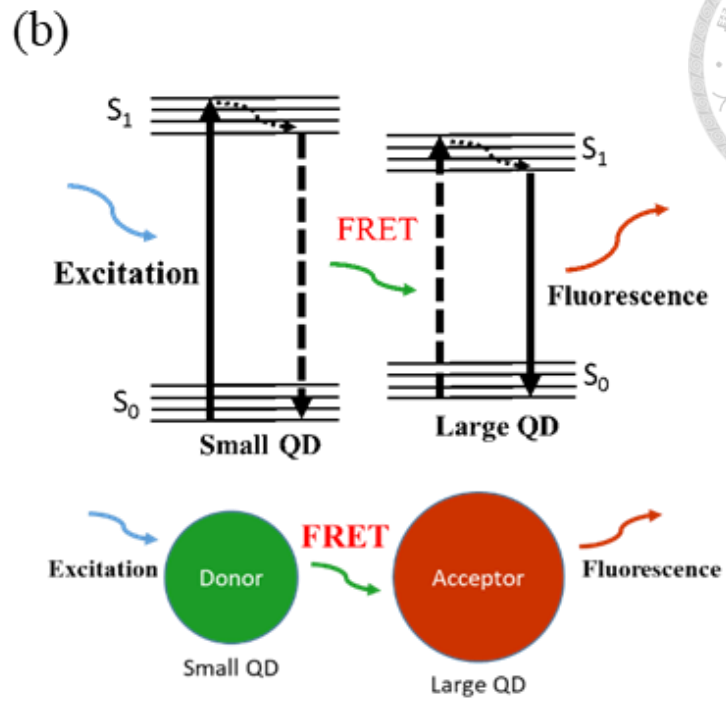


Fig. 3.12 (a) TRPL decay profiles of QD-PhCLED and QD-CLEDs. (b) Schematic of re-absorption and FRET process in QDs.

### 3.10 Summary



In this part, we show that the PhCLEDs integrated with QDs have higher blue-to-green conversion efficiency because of the FRET mechanism. In addition to radiative energy transfer channels, nonradiative energy transfer exists between QWs and QDs when QDs are in close contact with MQWs, which is called FRET. In E-O frequency response, QD-PhC-LED is 30% higher than QD-CLED-A in -3 dB bandwidth. Carriers in QD-PhC-LED can directly transfer energy through a nonradiative process. A higher -3dB frequency response is thus expected due to the direct carrier transport to the higher energy level of QDs. This result is also consistent with large-signal modulation. Finally, we observe that QD-PhC-LED has a slightly lower -3 dB bandwidth than QD-CLED-A when only discussing the light output of QDs. This result can be verified by TRPL measurement. Also, a thicker QD layer demonstrates a lower E-O frequency response because of its re-absorption and aggregation in QDs.

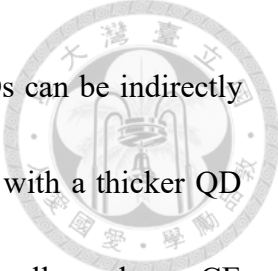
## Chapter 4. Conclusion



In our research, PhCLEDs and LEDs combined with QDs have both been explored and shown to have promising futures in the field of optical communication. We used PhCs nanohole structures in our LEDs to increase their modulation bandwidth. After integrated with QDs, PhCs structures also have the better performance in E-O frequency response. Here, we conclude our work as following two sections:

In the first part, we are investigating the potential of PhCLEDs to be used in a visible light communication system. Under small-signal modulation, PhCLEDs has achieved 178 MHz modulation bandwidth. Also, in order to demonstrate the immense potential of LEDs for use in VLC systems, a large-signal digitally modulated eye pattern was tested and exhibited at 400 Mbps by using OOK modulation.

In the second part, we conducted the E-O frequency response and OOK modulation measurements of the LEDs sprayed with QDs. When the overall blue and green light emission are benchmarked, devices with PhC nanoholes show a higher CE and a higher -3dB frequency response due to the occurrence of the direct carrier transport from QW to QDs, as compared with the QD-CLEDs. On the other hand, when only green light is considered by filtering out the blue color, the multi-path energy transfer to generate green color by QDs slows down the frequency response and degrades SNR in the eye diagram.



for the QD-PhCLED. Various energy transfer processes within QDs can be indirectly observed from TRPL and E-O frequency response. For the CLED with a thicker QD coating, the re-absorption process among QDs with various sizes as well as a lower CE deteriorate the frequency response. Our experimental results suggest the QD-PhCLED possesses a better bandwidth when both the blue and green light are employed for data transmission because of a higher light output intensity. On the other hand, if only converted light is used for data transmission, QD-PhCLED may not be favored due to multiple radiative and non-radiative energy transfer path, which increases the carrier lifetime.

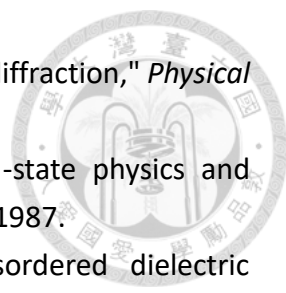
## Reference



- [1] M. F. Hossain, A. U. Mahin, T. Debnath, F. B. Mosharrof, and K. Z. Islam, "Recent research in cloud radio access network (C-RAN) for 5G cellular systems-A survey," *Journal of Network and Computer Applications*, vol. 139, pp. 31-48, 2019.
- [2] F. Deicke, W. Fisher, and M. Faulwaßer, "Optical wireless communication to ecosystem," in *2012 Future Network & Mobile Summit (FutureNetw)*, 4-6 July 2012 2012, pp. 1-8.
- [3] S. Rajbhandari *et al.*, "A review of gallium nitride LEDs for multi-gigabit-per-second visible light data communications," *Semiconductor Science and Technology*, vol. 32, no. 2, p. 023001, 2017.
- [4] A. Kerans, D. Vo, P. Conder, and S. Krusevac, "Pricing of spectrum based on physical criteria," in *2011 IEEE International Symposium on Dynamic Spectrum Access Networks (DySPAN)*, 2011: IEEE, pp. 223-230.
- [5] R. X. Ferreira *et al.*, "High bandwidth GaN-based micro-LEDs for multi-Gb/s visible light communications," *IEEE Photonics Technology Letters*, vol. 28, no. 19, pp. 2023-2026, 2016.
- [6] D. Tsonev *et al.*, "A 3-Gb/s Single-LED OFDM-Based Wireless VLC Link Using a Gallium Nitride  $\mu$  LED," *IEEE photonics technology letters*, vol. 26, no. 7, pp. 637-640, 2014.
- [7] H. Le Minh *et al.*, "100-Mb/s NRZ visible light communications using a postequalized white LED," *IEEE Photonics Technology Letters*, vol. 21, no. 15, pp. 1063-1065, 2009.
- [8] M. Meyns *et al.*, "Polymer-enhanced stability of inorganic perovskite nanocrystals and their application in color conversion LEDs," *ACS applied materials & interfaces*, vol. 8, no. 30, pp. 19579-19586, 2016.
- [9] N. Laurand *et al.*, "Colloidal quantum dot nanocomposites for visible wavelength conversion of modulated optical signals," *Opt. Mater. Express*, vol. 2, no. 3, pp. 250-260, 2012.
- [10] D. C. O. Brien, L. Zeng, H. Le-Minh, G. Faulkner, J. W. Walewski, and S. Randel, "Visible light communications: Challenges and possibilities," in *2008 IEEE 19th International Symposium on Personal, Indoor and Mobile Radio Communications*, 15-18 Sept. 2008 2008, pp. 1-5, doi: 10.1109/PIMRC.2008.4699964.
- [11] Y. Wang, Y. Wang, N. Chi, J. Yu, and H. Shang, "Demonstration of 575-Mb/s downlink and 225-Mb/s uplink bi-directional SCM-WDM visible light communication using RGB LED and phosphor-based LED," *Opt. Express*, vol. 21,



- no. 1, pp. 1203-1208, 2013/01/14 2013, doi: 10.1364/OE.21.001203.
- [12] B.-R. Hyun, C.-W. Sher, Y.-W. Chang, Y. Lin, Z. Liu, and H.-C. Kuo, "Dual Role of Quantum Dots as Color Conversion Layer and Suppression of Input Light for Full-Color Micro-LED Displays," *The Journal of Physical Chemistry Letters*, vol. 12, no. 29, pp. 6946-6954, 2021/07/29 2021, doi: 10.1021/acs.jpcclett.1c00321.
- [13] Y. Wu, J. Ma, P. Su, L. Zhang, and B. Xia, "Full-Color Realization of Micro-LED Displays," *Nanomaterials*, vol. 10, no. 12, p. 2482, 2020. [Online]. Available: <https://www.mdpi.com/2079-4991/10/12/2482>.
- [14] X. Li *et al.*, "Highly stable CsPbBr<sub>3</sub> quantum dots by silica-coating and ligand modification for white light-emitting diodes and visible light communication," *Chemical Engineering Journal*, vol. 419, p. 129551, 2021.
- [15] C. Foucher *et al.*, "Flexible glass hybridized colloidal quantum dots for Gb/s visible light communications," *IEEE Photonics Journal*, vol. 10, no. 1, p. 1c11, 2018.
- [16] X. Xiao *et al.*, "Improving the modulation bandwidth of LED by CdSe/ZnS quantum dots for visible light communication," *Opt. Express*, vol. 24, no. 19, pp. 21577-21586, 2016/09/19 2016, doi: 10.1364/OE.24.021577.
- [17] S. Mei *et al.*, "High-Bandwidth White-Light System Combining a Micro-LED with Perovskite Quantum Dots for Visible Light Communication," *ACS Applied Materials & Interfaces*, vol. 10, no. 6, pp. 5641-5648, 2018/02/14 2018, doi: 10.1021/acsami.7b17810.
- [18] X. Liu *et al.*, "White-Light GaN- $\mu$ s LEDs Employing Green/Red Perovskite Quantum Dots as Color Converters for Visible Light Communication," *Nanomaterials*, vol. 12, no. 4, p. 627, 2022. [Online]. Available: <https://www.mdpi.com/2079-4991/12/4/627>.
- [19] S. Chanyawadee *et al.*, "Increased color-conversion efficiency in hybrid light-emitting diodes utilizing non-radiative energy transfer," *Advanced Materials*, vol. 22, no. 5, pp. 602-606, 2010.
- [20] T.-C. Lin *et al.*, "Large-signal modulation performance of light-emitting diodes with photonic crystals for visible light communication," *IEEE Transactions on Electron Devices*, vol. 65, no. 10, pp. 4375-4380, 2018.
- [21] Y. F. Yin, W. Y. Lan, T. C. Lin, C. Wang, M. Feng, and J. J. Huang, "High-Speed Visible Light Communication Using GaN-Based Light-emitting Diodes With Photonic Crystals," *Journal of Lightwave Technology*, vol. 35, no. 2, pp. 258-264, 2017, doi: 10.1109/JLT.2016.2634005.
- [22] Y.-H. Lin, T.-C. Lin, C.-H. Cheng, H.-C. Kuo, J.-J. Huang, and G.-R. Lin, "Photonic crystal structured blue  $\mu$ sLED with aperture size dependent data transmission performance in plastic fiber link," *OSA Continuum*, vol. 3, no. 1, pp. 104-119, 2020/01/15 2020, doi: 10.1364/OSAC.378277.

- 
- [23] K. Ohtaka, "Energy band of photons and low-energy photon diffraction," *Physical Review B*, vol. 19, no. 10, p. 5057, 1979.
- [24] E. Yablonovitch, "Inhibited spontaneous emission in solid-state physics and electronics," *Physical review letters*, vol. 58, no. 20, p. 2059, 1987.
- [25] S. John, "Strong localization of photons in certain disordered dielectric superlattices," *Physical review letters*, vol. 58, no. 23, p. 2486, 1987.
- [26] E. Istrate and E. H. Sargent, "Photonic crystal heterostructures and interfaces," *Reviews of modern physics*, vol. 78, no. 2, p. 455, 2006.
- [27] S. T. M. Fryslie, M. P. T. Siriani, D. F. Siriani, M. T. Johnson, and K. D. Choquette, "37-GHz modulation via resonance tuning in single-mode coherent vertical-cavity laser arrays," *IEEE Photonics Technology Letters*, vol. 27, no. 4, pp. 415-418, 2014.
- [28] C. Wiesmann, K. Bergeneck, N. Linder, and U. Schwarz, "Analysis of the emission characteristics of photonic crystal LEDs," in *Photonic Crystal Materials and Devices VIII*, 2008, vol. 6989: SPIE, pp. 118-126.
- [29] Y.-F. Yin, W.-Y. Lan, Y.-H. Hsu, Y.-F. Hsu, C.-H. Wu, and J. Huang, "High-speed modulation from the fast mode extraction of a photonic crystal light-emitting diode," *Journal of Applied Physics*, vol. 119, no. 1, p. 013103, 2016.
- [30] C. Xu, X. Liu, L. F. Mollenauer, and X. Wei, "Comparison of return-to-zero differential phase-shift keying and on-off keying in long-haul dispersion managed transmission," *IEEE photonics technology letters*, vol. 15, no. 4, pp. 617-619, 2003.
- [31] K. C. Majhi and M. Yadav, "Chapter 5 - Synthesis of inorganic nanomaterials using carbohydrates," in *Green Sustainable Process for Chemical and Environmental Engineering and Science*, Inamuddin, R. Boddula, M. I. Ahamed, and A. M. Asiri Eds.: Elsevier, 2021, pp. 109-135.
- [32] G. J. Supran *et al.*, "QLEDs for displays and solid-state lighting," *MRS bulletin*, vol. 38, no. 9, pp. 703-711, 2013.
- [33] X. Lian, M.-Y. Wei, and Q. Ma, "Nanomedicines for near-infrared fluorescent lifetime-based bioimaging," *Frontiers in Bioengineering and Biotechnology*, vol. 7, p. 386, 2019.
- [34] A. P. Alivisatos, "Semiconductor clusters, nanocrystals, and quantum dots," *science*, vol. 271, no. 5251, pp. 933-937, 1996.
- [35] A. Litvin, I. Martynenko, F. Purcell-Milton, A. Baranov, A. Fedorov, and Y. Gun'ko, "Colloidal quantum dots for optoelectronics," *Journal of Materials Chemistry A*, vol. 5, no. 26, pp. 13252-13275, 2017.
- [36] J. Caruge, J. E. Halpert, V. Wood, V. Bulović, and M. Bawendi, "Colloidal quantum-dot light-emitting diodes with metal-oxide charge transport layers," *Nature photonics*, vol. 2, no. 4, pp. 247-250, 2008.
- [37] G. A. Jones and D. S. Bradshaw, "Resonance energy transfer: from fundamental

- theory to recent applications," *Frontiers in Physics*, vol. 7, p. 100, 2019.
- [38] R. Nelz *et al.*, "Near-Field Energy Transfer between a Luminescent 2D Material and Color Centers in Diamond," *Advanced Quantum Technologies*, vol. 3, no. 2, p. 1900088, 2020.
- [39] F. Zhang *et al.*, "Nonradiative energy transfer between colloidal quantum dot-phosphors and nanopillar nitride LEDs," *Opt. Express*, vol. 20, no. 102, pp. A333-A339, 2012.
- [40] J. Hottechamps, T. Noblet, A. Brans, C. Humbert, and L. Dreesen, "How Quantum Dots Aggregation Enhances Förster Resonant Energy Transfer," *ChemPhysChem*, vol. 21, no. 9, pp. 853-862, 2020, doi: <https://doi.org/10.1002/cphc.202000067>.
- [41] Y.-P. Chen *et al.*, "Combined effects of surface plasmon coupling and Förster resonance energy transfer on the light color conversion behaviors of colloidal quantum dots on an InGaN/GaN quantum-well nanodisk structure," *Nanotechnology*, vol. 32, no. 13, p. 135206, 2021/01/08 2021, doi: [10.1088/1361-6528/abd05e](https://doi.org/10.1088/1361-6528/abd05e).
- [42] C.-Y. Liu *et al.*, "Color-conversion efficiency enhancement of quantum dots via selective area nano-rods light-emitting diodes," *Opt. Express*, vol. 24, no. 17, pp. 19978-19987, 2016/08/22 2016, doi: [10.1364/OE.24.019978](https://doi.org/10.1364/OE.24.019978).